COMPUTER MODELING OF SINTERING IN CERAMICS

by

Alice C. De Bellis

B.S. in Engineering Mechanics, The Johns Hopkins University, May 1989

Submitted to the Graduate Faculty of

The School of Engineering in partial fulfillment

of the requirements for the degree of

Master of Science in Mechanical Engineering

University of Pittsburgh

2002

UNIVERSITY OF PITTSBURGH

SCHOOL OF ENGINEERING

This thesis was presented

by

Alice Cleveland De Bellis

It was defended on

June 20, 2002

and approved by

Patrick Smolinski, Associate Professor,
Department of Mechanical Engineering

Ian Nettleship, Associate Professor, Department of
Materials Science and Engineering

Thesis Advisor: William S. Slaughter, Associate
Professor, Department of Mechanical Engineering

ABSTRACT

COMPUTER MODELING OF SINTERING IN CERAMICS

Alice C. De Bellis, M.S.

University of Pittsburgh, 2002

A computer model of the sintering process has been developed to study the evolution of the microstructure in a sintered part as a function of the volumetric density. The model of the sintering process begins with a particle packing model, which generates a close-packed array of particles. A Representative Volume Element (RVE) of the packing is selected and examined. Next is densification, which is simulated by uniformly increasing the radii of the particles.

Two dimensionless parameters, the intercept ratio Λ and the surface area ratio Ψ, are used to quantify the model. This model shows good results at lower packing densities. Areas in which the model can be improved and extended are also highlighted.

The intent of this model is to predict the final microstructure of a sintered part based on its geometry and its stereology. It treats the sintering process as continuous, without the stages normally used to describe sintering.

KEYWORDS

Sintering

Particle packing

Powder metallurgy

Dimensionless parameters

Densification

Microstructure

Modeling

Stereology

ACKNOWLEDGEMENTS

I would like to thank my adviser, Dr. William Slaughter, for his guidance and support in this endeavor. I would also like to thank Dr. Ian Nettleship of the Materials Science and Engineering Department, for helping me understand the sintering process, and fellow graduate students Jesus Ameneiro and Rich McAfee for their encouragement and assistance. Finally, many thanks to Kumar Krishnan for providing the foundation on which I could build.

This work is dedicated to my husband Michael.

TABLE OF CONTENTS

LIST OF TABLES

LIST OF FIGURES

1.0 INTRODUCTION

1.1 Sintering

Sintering is a manufacturing process in which a fine powder that has been formed into a shape is subsequently fired at high temperatures. The compact, when fired, densifies and becomes non-porous. More formally, sintering is a thermal treatment that bonds particles together into a solid, coherent structure, by means of mass transport mechanisms occurring largely at the atomic level [1]. Sintering can occur either at atmospheric pressure or under isostatic or hydrostatic pressure. It generally takes place at temperatures in excess of half the absolute melting temperature. If sintering takes place at temperatures high enough that some melting occurs, it is called liquid-phase sintering; sintering that takes place at lower temperatures is called solid-state sintering.

Sintering is an inexpensive way of making parts, provided the finished part can be used as is and does not require additional machining. The difficulty is that, when a part is sintered, its size and shape change non-linearly, which needs to be taken into account by the designer of the unfired piece. At present, the only practical way of doing this is by trial and error; e.g., by making prototype shapes until a suitable mold shape has been identified. While this may be acceptable for very high-volume items, it is not cost-effective for small batches.

Various models have been developed for the sintering process. Ashby [2] developed sintering diagrams, which consider the influence of various mass-transport mechanisms during various stages of the sintering process. This approach is strongly dependent on the material properties of the sintered compact.

Another model, developed by Aigeltinger and DeHoff [3], attempts to predict microstructural changes in terms of the geometric properties of features of the sintered microstructure. This model is described in more detail in Section 3.0.

The intent of this work is to develop a model that will predict the microstructural properties of a sintered part based on its geometric properties. Specifically, the model uses dimensionless length and area ratios of the sintered part to predict its microstructure, which allows comparisons of microstructures with different length scales. This model has two advantages over previous models:

- Because it uses dimensionless parameters, the results of experiments with different length scales can be compared directly,
- Because it does not consider the material properties of the sintered part, results from this model can be generalized to different materials and different types of materials.

The sintering process has been used throughout history. The ancient Egyptians sintered metal and ceramics as far back as 3000 B.C. [1]. Today, sintering is used to manufacture a wide range of products, including rocket nozzles, nuclear fuel elements, golf clubs and porcelain plumbing fixtures.

1.2 The Sintering Process

1.2.1 Driving Energy and Mass-Transport Mechanisms

The initial powder (called a green compact) has a large surface area relative to its volume. This surface area provides the driving force in sintering, which is the reduction of free surface energy resulting from the high surface area of the particles [4].

Sintering proceeds from various mass-transport mechanisms. These can be divided into surface transport and bulk transport mechanisms. In surface transport mechanisms, atoms move from the surface of one particle to the surface of another particle. In bulk transport mechanisms, atoms move from the particle interior to the surface. Surface transport mechanisms lead to neck growth without shrinkage or densification, while bulk transport mechanisms result in net particle movement, leading to shrinkage and densification. Densification means an increase in packing density, as defined in Section 1.3.

This thesis does not provide exhaustive detail about mass-transport mechanisms during sintering. For further detail, the reader is referred to references [1] and [5].

The surface transport mechanisms are surface diffusion and vapor transport, and the bulk transport mechanisms are lattice diffusion, grain boundary diffusion, and viscous flow. In powders composed of different materials, chemical reactions (also called reactive processes) may also provide additional mass-transport mechanisms [1].

Different mechanisms dominate at different points in the sintering process, and different materials exhibit different mechanisms. For instance, viscous flow is the dominant mechanism when sintering amorphous materials, while grain boundary diffusion (obviously) plays no part. The opposite is generally true for crystalline materials. In liquid-phase sintering (which is not discussed here), viscous flow and related mechanisms play a significant role.

Sintering may occur at atmospheric pressure, under isostatic or hydrostatic pressure. This pressure-assisted sintering increases the sintering rate, reduces sintering time, and reduces porosity in the final part.

The sintering process has historically been divided into four stages. These are described in Table 1 [1].

Table 1. The Classic Stages of Sintering.

Stage	Process	Surface Area Loss	Densification	Coarsening
Adhesion	Contact formation	Minimal, unless compacted at high pressures	None	None
Initial	Neck growth	Significant, up to 50% loss	Small at first	Minimal
Intermediate	Pore rounding and elongation	Near total loss of open porosity	Significant	Increase in grain size and pore size
Final	Pore closure, final densification	Negligible further loss	Slow and relatively minimal	Extensive grain and pore growth

A sintered part begins as a compact, which is a powder placed into a mold or die cavity. The green compact is low-density, inhomogeneous and porous, and generally lacking in physical integrity. There is, however, a small degree of adhesion between adjacent particles.

As the compact is heated, necks begin to form at the contacts between the particles, driven by the high surface energy of the particles. See Figure 1.

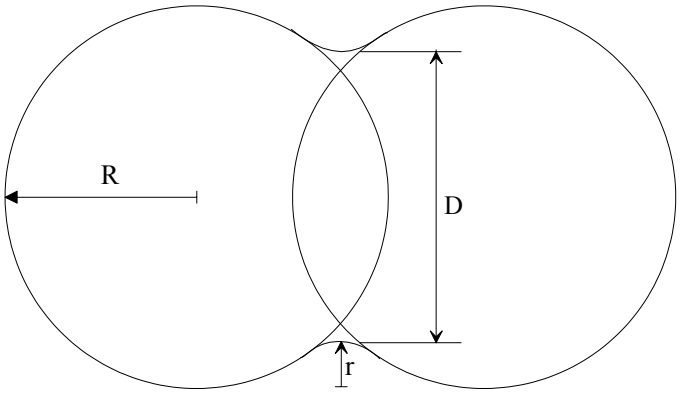

Figure 1. Neck Formation.

Initial neck formation is driven by the stress gradient resulting from the different curvatures of the particle and the neck [5]. This is governed by the Laplace equation, namely

$$\sigma = \gamma\left(\frac{1}{r_1} + \frac{1}{r_2}\right)$$

Where γ is the surface energy and r_1 and r_2 are the radii of curvatures of the two surfaces. In the case illustrated by Figure 1, this reduces to

$$\sigma = \gamma\left(\frac{1}{R} - \frac{1}{r}\right)$$

The minus sign results because the two surfaces are curved in opposite directions. At the beginning of neck growth the stress gradient is high, when the neck radius r is small, and decreases as the neck thickens.

Bulk transport mechanisms result from movement of atoms along grain boundaries and through the lattice to the surface. This results in an increase in the contact area between particles, and a corresponding increase in the total amount of grain boundary and decrease of surface area. Densification results from bulk transport mechanisms.

Sintering can be divided into three stages, which are listed in Table 1. These are called initial neck growth, intermediate stage sintering and final stage sintering. This division reflects differences in geometry during the sintering process; also, as stated previously, different mass-transport mechanisms dominate during the different stages.

1.2.2 Initial Neck Growth

In this initial phase of sintering, necks begin to form at the contact points between adjacent particles (see Figure 1). Neck formation is driven by the energy gradient resulting from the different curvatures of the particles and the neck, as discussed in Section 1.2.1. Surface diffusion is usually the dominant mass-transport mechanism during the early stages of neck growth, as the compact is heated to the sintering temperature.

1.2.3 Intermediate Stage Sintering

Intermediate phase sintering begins when adjacent necks begin to impinge upon each other. This occurs when the quantity $\frac{D}{2R} \approx 0.3$ [1] (see Figure 1). Densification and grain growth occur during this stage.

The packing density and coordination number of the green packing are important during this stage. A high green packing density produces rapid sintering with relatively few pores in the final object. Very low green packing densities (around 40%), which are also associated with low coordination numbers, can lead to coarsening (increase in mean grain size) without densification (decrease in porosity). In extreme cases, this may lead to open-pore structures lacking in structural integrity [1]. See Figure 2.

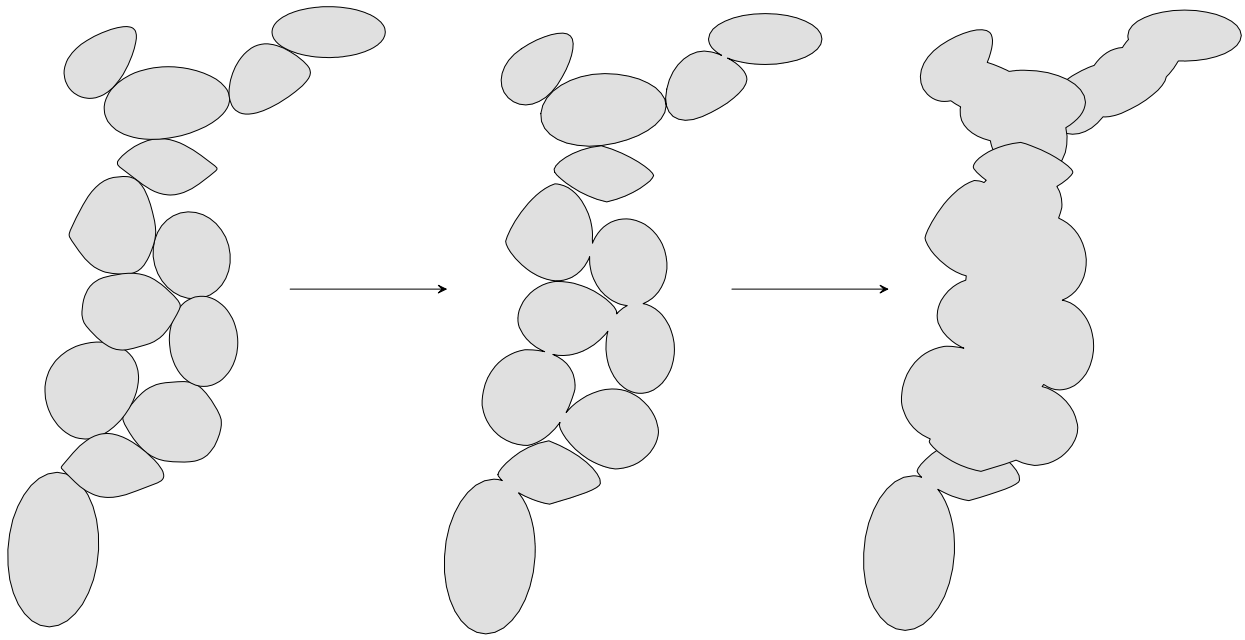

Figure 2. Coarsening Resulting from Low Coordination Number.

During intermediate stage sintering, grains begin to form from the individual particles, and the material's final grain structure begins to develop. Pore networks form along the grain boundaries. At the beginning of the intermediate stage, the pores form a network of interconnected cylindrical pores broken up by necks. By the end, the pores are smoother and begin to pinch off and become isolated from each other.

Bulk transport mechanisms, such as grain boundary diffusion and volume diffusion, dominate the sintering process during this stage. As stated previously, these bulk transport mechanisms cause material to migrate from inside the particles to the surface, resulting in contact flattening and densification.

1.2.4 Final Stage Sintering

Final stage sintering begins when most of the pores are closed. As sintering proceeds, the pores, which during intermediate stage sintering form a network, have become isolated from each other.

Final stage sintering is much slower than the initial and intermediate stages. As grain size increases, the pores tend to break away from the grain boundaries and become spherical. Smaller pores are eliminated, while larger pores can grow, a phenomenon called Ostwald ripening. In some cases, pore growth during final stage sintering can lead to a decrease in density, as gas pressure in the larger pores tends to inhibit further densification. This can be mitigated by having the final stage sintering occur in a partial vacuum.

1.3 Measurement Techniques

1.3.1 Definitions

In a sintered part or compact, packing density is the fraction of the space in the green compact that is occupied by the material being sintered. A packing density of 0.79 means that 79% of the space is occupied by the material. The remaining space (0.21, or 21% in this example) is the porosity. Packing density is sometimes called volumetric density. The packing density is different from the "true" density (mass per unit volume), which is a material property. Packing density is a function of the geometry of the compact or sintered part. Packing density may also be called volumetric density or solid volume fraction, and is abbreviated here as V_V^S [6].

In this document, the term "density" implies "packing density" unless otherwise noted. A detailed discussion of measurement techniques for packing density and porosity is given in [1].

1.3.2 Stereology

Stereology is a method of analyzing the structure of a three-dimensional solid from the information provided by a two-dimensional plane section taken through the solid. It is a spatial version of sampling theory [7].

Structures and lengths of a solid are measured by slicing through the solid, polishing the exposed surface, etching it with acid and examining it under a microscope. A number of techniques are used to determine the various quantities of interest. This thesis reviews a number of common techniques; for a detailed study of the field of quantitative microscopy, the reader is referred to [8].

1.3.2.1 Calculating the Packing Density

The packing density (or alternately, porosity) can be measured using a test grid, as shown in Figure 3 [1]. The packing density is the fraction of points in the test grid that are inside any of the particles, and the porosity is the fraction of points in the test grid that are not inside any of the particles.

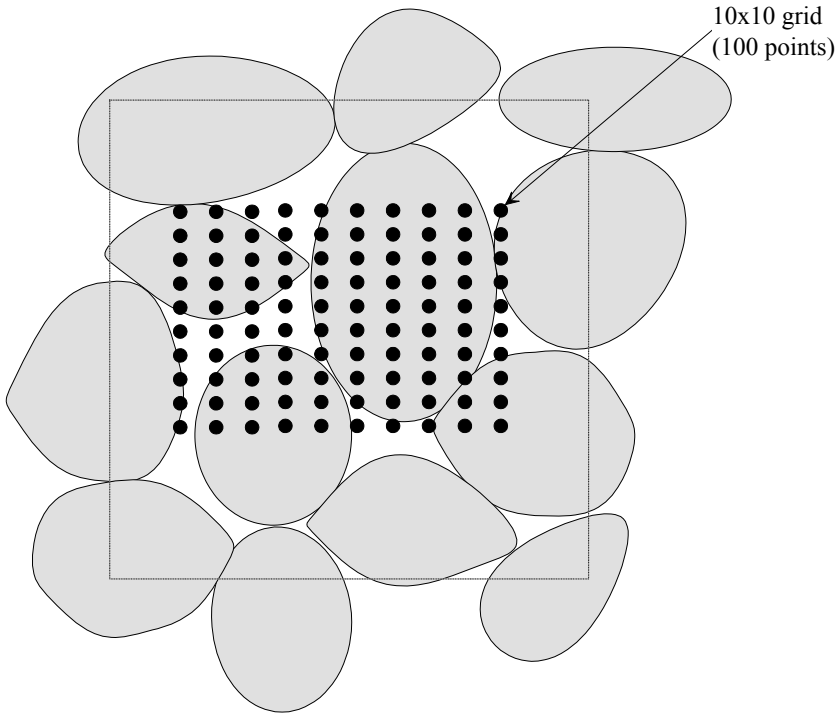

Figure 3. Calculating the Packing Density.

1.3.2.2 Calculating the Grain Size

The pore size and grain size can be estimated using a number of different techniques. The random intercept method calculates the mean grain size of spherical grains by drawing a test line across the surface, and counting the number of intersection s per unit length of test line N_L and the number of features per unit cross-sectional area N_A:

$$G = \frac{4}{\pi}\frac{N_L}{N_A}$$

This method, though simple enough, is problematic. Because the slices are taken through the microstructure at random, the grain size measured this way will be smaller than the actual grain size. In addition, the grains are not usually spherical. A better measurement technique is to compute the mean intercept size L. L is the ratio of the fractional density V_S to the number of grain (or pore) intercepts per unit length:

$$L = \frac{V_S}{N_L}$$

This is illustrated in Figure 4 [1].

If grain size distribution is important, the mean intercept size can be calculated for multiple slices at different orientations.

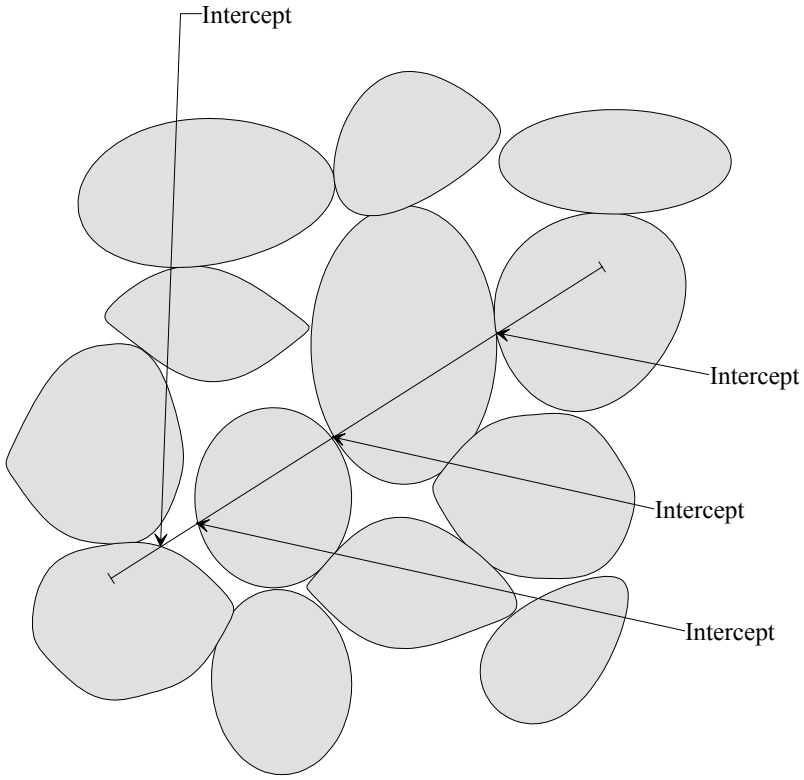

Figure 4. Calculating the Mean Intercept Size.

1.3.3 Internal Surface Area Parameters

This analysis uses two additional parameters to characterize the microstructure. These are the solid-solid surface area S_V^{SS} and the solid-void surface area S_V^{SV}. The solid-solid surface area is the contact area between adjacent particles, and the solid-void surface area is the surface area of the pores. These quantities are used to define the dimensionless parameters described in the following section.

1.3.4 Dimensionless Parameters

The quantities defined in the preceding sections are dimensional (i.e., length, grains per unit area, etc.). This makes it difficult to compare quantities among microstructures with different length scales. It would be convenient to define dimensionless quantities, which would allow direct comparisons among microstructures with different length scales. Two such quantities have been defined: these are the ratio of the solid-solid and solid-void surface area Ψ, called the surface area ratio, and the ratio of the mean grain and mean void intercepts Λ, called the intercept ratio [6]. These are defined by

$$\Lambda = \frac{V_V^S S_V^{SV}}{(1-V_V^S)(S_V^{SV} + 2S_V^{SS})}$$

and

$$\Psi = \frac{S_V^{SS}}{S_V^{SV}}$$

Where S_V^{SV} is the solid-void surface area, S_V^{SS} is the solid-solid surface area, and V_V^S is the packing or volumetric density. These quantities are used to evaluate the model described in Section 4.0.

2.0 PARTICLE PACKING

The characteristics of the green packing are important in the sintering process. Various models are considered, for mono-sized particles, binary mixtures and continuously distributed particle sizes, and for spherical and non-spherical particles.

2.1 Particle Shapes

In nature, particles are never exactly spherical. However, geometrically, spheres are the easiest particle shape to model, as they can be defined by a minimum number of parameters (coordinates of center plus radius), and are symmetrical and isotropic. Smith and Midha [9] have employed an approach in which individual particles are constructed as an agglomeration of spheres, while Nandakumar et al [10] have modeled cylindrical particles. However, spheres are still the preferred shape for most models. Non-spherical particles are difficult to model geometrically; for instance, if flakes (coin-shaped particles) or rods (cylindrical particles) are used, their orientation as well as their location must be considered. This vastly increases the amount of computing time required to model the packing, and was not considered feasible for this project. The following discussion considers only spherical particles.

The highest theoretical packing density of mono-sized spherical particles occurs with a close-packed arrangement, either a hexagonal-close-packed (hcp) or a face-centered cubic (fcc) configuration. The theoretical packing density for these configurations is 0.74 [11]. Actual packing densities are usually lower. The highest theoretical coordination number also occurs in an hcp or fcc configuration, with coordination numbers of 12 [11].

2.2 Particle Size Distributions

Particle size distribution has a significant effect on the sintering process and on the microstructure of the sintered part [12-14]. A wider distribution of particle sizes produced a higher green density and faster sintering in both ceramics (alumina) [15] and metals (tungsten) [13]. Ting and Lin [16, 17] have found that sintering kinetics in alumina depend on the initial particle distribution.

Three different types of particle size distribution are discussed in the literature. These are mono-dispersed spheres, binary mixtures of spheres, and spheres following a continuous log-normal distribution.

2.2.1 Mono-Dispersed Spheres

Packings of mono-dispersed spheres, while not representative of real-life particle packing situations, are the easiest to model. Such packings can be modeled at a macroscopic scale, using ball bearings or similar objects, allowing a computer model of such a packing to be checked against an experimental model [18]. However, this model, besides not being very representative of a real packing, does not produce high packing densities; Smith and Midha [19] report that packing densities in excess of 0.64 cannot be achieved with a random mono-dispersed packing, despite the higher theoretical packing densities of close-packed arrangements. Smith and Midha define a random packing as "an arrangement of spheres which has as high a fractional density as possible without the formation of long-range order within the assembly, such as a face-centered cubic arrangement." Their experimental results with a vibrated powder of mono-sized bronze spheres of diameters 850 – 853 μm bear this out. Matheson [18] also reports that a shaken stack of ball bearings packs to a density of 0.6366.

This low packing density is a result of the fact that a random mono-dispersed packing will tend to form bridging structures, as shown in Figure 5 [11]. The highest particle in this example is gravitationally stable, but it is not in the lowest-energy configuration available to it, because the particles supporting it do not permit it to move down. This leaves a large gap beneath it.

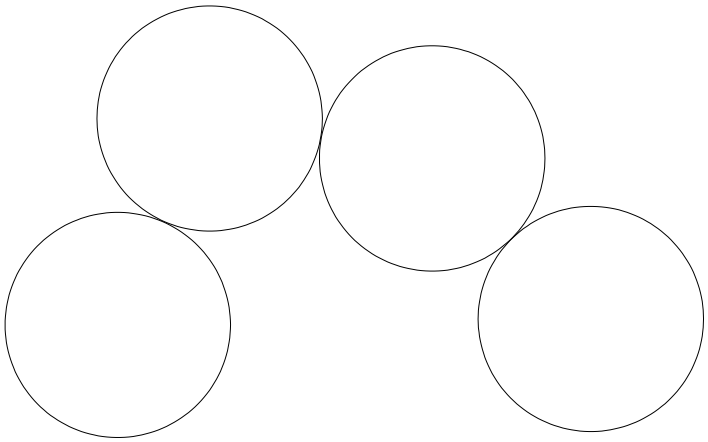

Figure 5. Formation of Bridging Structures in a Random Packing.

2.2.2 Binary Mixtures

If smaller particles are introduced into a packing of mono-dispersed particles, it becomes a binary mixture. The smaller particles serve to fill the inter-particle gaps in the original packing and increase the overall packing density, as shown in Figure 6. In order to do this, the new particles must be significantly smaller than the original particles, small enough to fit in the pores left among the larger particles. Smith and Midha [19] report that packing density increases for particle size ratios greater than 2.

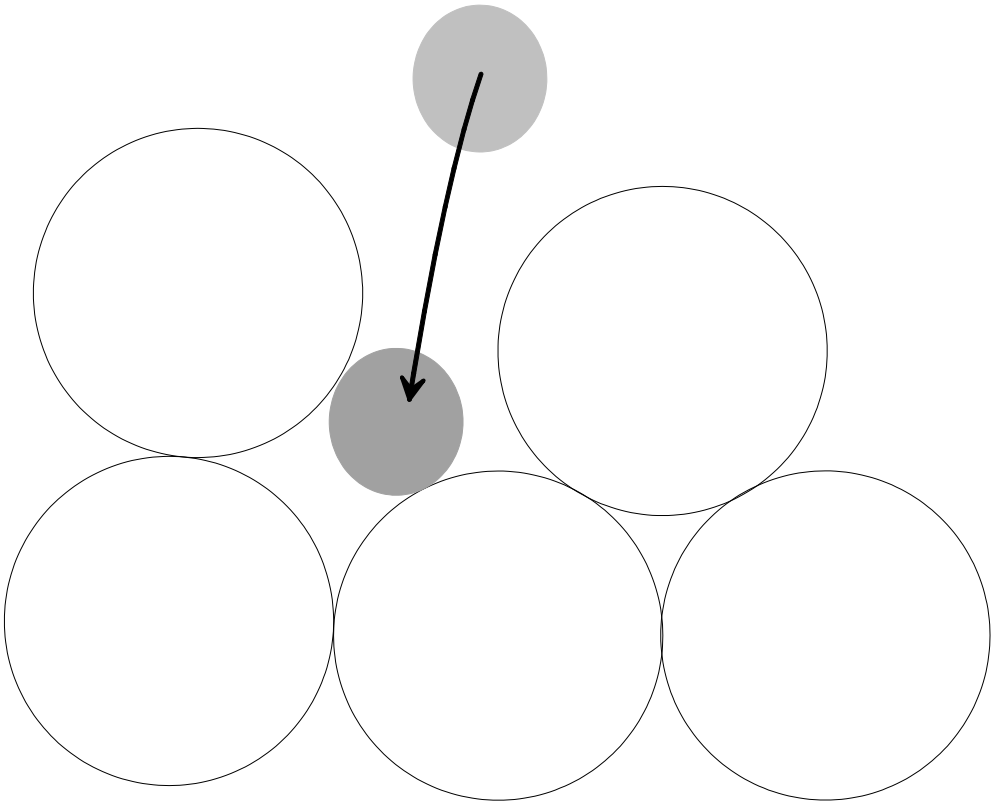

Figure 6. Binary Mixture of Powders.

Binary mixtures overcome some of the limitations of mono-dispersed packings, and sinter more efficiently; that is, there is less variation in pore sizes and the pores are distributed more uniformly throughout the sintered part [20]. However, they still do not represent a realistic packing arrangement. According to German [21], most particle powders obey a log-normal distribution.

2.2.3 Log-Normal Distribution

Spherical particles obeying a log-normal distribution are defined by [22]

$$P(r) = \frac{1}{r\sigma\sqrt{2\pi}} e^{\frac{-(\ln(r)-\mu)^2}{2\sigma^2}}$$

Where r is the radius of the sphere, σ is the standard deviation and μ is the mean of the distribution. The particles used to model the sintering process in this analysis follow a log-normal distribution. Patterson et al [12, 13] have examined a number of log-normal distributions, and found that distributions with larger values of σ tended to densify more rapidly.

Refer to Appendix B for more information about the log-normal distribution and its applicability to particle packing models.

2.3 Particle Packing Models

Particle packing models involve more than the selection of an appropriate size distribution. The mechanics of arranging the particles must be considered as well. The relationship between green densities and sintering have been studied by Zheng and Reed [23]. The properties of the green compact are critical to the final microstructure of the sintered part, so a great deal of attention was given to the selection of a suitable particle packing model. Most sintering models use ordered arrays of spheres or polyhedra [1]; this model uses a random arrangement.

Regardless of the particle size distribution, computer models of particle packing can be divided into several categories. Particles can be deliberately stacked in an array, they can be dropped from a height, or they can be generated randomly in a selected volume and rearranged to a stable non-overlapping configuration.

In the "dropping" model, individual particles are dropped from a height into a virtual container. When the particle contacts another particle, it can either roll off it until it reaches some suitable minimum height, or settle into a stable configuration where it lands. This approach is described by Edwards [24] for both mono-dispersed and poly-dispersed spheres, and

Nandakumar [10] discusses it for mono-dispersed spherical and cylindrical particles. In the "stacking" model, individual particles are generated in specific locations relative to each other, to form a stable array. This approach is described by Krishnan [25] for log-normally distributed particles. Finally, in the "random generation" model, all particles are generated in a volume of space, then rearranged to form a stable, non-overlapping array. This approach is described by Nolan and Kavanagh for mono-dispersed and log-normally distributed particles [11, 26].

The "dropping" model has the advantage of most closely replicating the physical process of pouring a powder into a mold. Computationally, however, it is a dynamic process and is therefore harder to model, requiring that particle movement be taken into account. The "stacking" model will create a very nice packing; however, it lacks randomness.

The "random generation" model, which was chosen for this simulation, produces a well-mixed packing. It also has the advantage of considering the packing as static at each step of the rearrangement, which eliminates some of the problems with the dynamic approach described above. The rearrangement can be achieved in one of two ways:

1. Start with the particles far apart (not touching at all), and move them closer together.

2. Start with the particles close together (overlapping), and move them apart.

The second option was chosen for this model. The overlapping particles are pushed apart with a force proportional to the overlap. The advantage of this approach is that relatively little particle movement is required to produce a stable close packing. It also ensures that the packing remains in the same region of space after rearrangement. This is convenient when selecting a Representative Volume Element (RVE), as described in Section 4.2. This is

explained in further detail in [26]. Details of the rearrangement algorithms are given in Appendix A.

3.0 PREVIOUS SINTERING MODELS

Much work has been done in developing sintering models. According to Exner [27], modern attempts to quantitatively define the sintering mechanisms date from the 1940s. Since that time, many aspects of sintering kinetics, geometry and driving forces have been worked out. A review of the history of sintering models is provided by [27].

Some attempts have been made to predict the final microstructure based on the geometric properties of the initial packing. Aigeltinger and DeHoff [3] have attempted to describe the microstructural pathways (path of microstructural change) in terms of geometric properties of features of the sintered microstructure. They examined topological properties, including pore-solid interface, and metric properties, including solid-void fraction and total curvature of the pore-solid interface. The process was used to study sintering in three different copper powders: two spherical powders and a dendritic powder. The results for the two spherical powders were qualitatively similar, suggesting that the two powders follow paths that are qualitatively similar, differing only in scale.

This model has the advantage of not making simplifying assumptions about the geometry or the microstructure. However, measuring the topological properties in this model is a very labor-intensive process, requiring that the experimenters take a large number of closely-spaced sections through the part and compare them.

A geometric model developed by Slaughter and Nettleship [6, 28, 29] attempts to predict the final microstructure of a sintered part using dimensionless parameters.

Slaughter [6] defines the nondimensional parameters Λ and Ψ, which are defined in Section 1.3.4. These parameters allow microstructures with different length scales to be compared. This facilitates comparisons between models and experimental data. The use of these parameters is illustrated in [6] for a number of different packing models, and for experimental data. This model was later extended by Krishnan [25] to a distributed packing.

4.0 DESCRIPTION OF MODEL

This model hypothesizes that the final microstructure of a sintered part can be predicted from its geometric properties. Eventually, such a model could allow the final shape of a sintered part to be predicted from the geometry of its green packing.

This model is an attempt to build on the work done previously by Slaughter, Nettleship and Krishnan, as described in Section 3.0. The model used for this thesis considers only the geometric properties of the packing. It treats the packing as an array of spherical particles whose radii obey a log-normal distribution.

One drawback to Krishnan's model is that the packing density of the green compact is low, on the order of 40%. As described in Section 2.2, this is low even for a mono-dispersed packing. The current model creates an initial packing with a much higher green density, on the order of 65%.

The model proceeds in three stages: generating the initial packing, rearranging it into a stable, non-overlapping configuration, and densifying it. The algorithms used to generate, rearrange, densify and measure the packing are described in detail in Appendix A.

4.1 Initial Packing and Rearrangement

The initial packing and rearrangement is based on work previously done by Nolan and Kavanagh [11, 26]. The packing and rearrangement algorithm is the one described as "random generation" in Section 2.3. The particles are spherical, and the radii are log-normally distributed with a mean $\mu = 0.0026$ and a standard deviation $\sigma = 0.0016$[*]. These values were chosen for two

[*] All units used to describe the model are based on arbitrary distance units (e.g., length, length squared, etc.) unless otherwise noted.

reasons. First, as the model was being developed, it was decided to model relatively small particles. A maximum length scale for the total packing (that is, the Representative Volume Element) of one was chosen. This choice was arbitrary; it was based more on mathematical elegance than any physical basis. However, because the quantities being examined in the analysis are dimensionless, other values could be chosen. The concept of the Representative Volume Element is discussed in Section 4.2. Second, Nolan and Kavanagh [26] define the dimensionless absolute standard deviation as (σ/μ). They found that packings with a high absolute standard deviation packed more efficiently. Good results were seen for values of (σ/μ) around 6; the absolute standard deviation for this packing is 0.62.

The initial packing and rearrangement proceeds as follows. A number of particles are generated in space. The nearest neighbors of each particle are identified, and the packing statistics (mean overlap among all particles, mean coordination number, fraction of particles in a gravitationally stable arrangement) are computed.

To rearrange the packing, the program considers each particle in turn. It computes the overlap between it and its neighbors, and moves it in such a way as to minimize the overlap. The particle may be moved by simple translation, by rolling it around its neighbors, or by a combination of these mechanisms. At each step, the packing statistics are recomputed. This rearrangement proceeds until the mean overlap of the packing is below a selected value (one-sixth of the mean particle radius) and the fraction of particles in a gravitationally stable configuration is above a selected value (75%). This is explained in further detail in Appendix A.

4.2 Selection of Representative Volume Element (RVE)

Once the packing has been rearranged, most of the particles are clustered around the origin, as shown in Figure 7. The particles are densely packed around the origin; in regions far from the origin, the packing is less dense. In order to ensure that the model represents a dense packing, a Representative Volume Element (RVE) is selected. Physically, this RVE represents an arbitrarily selected volume within the sintered part. The RVE used in this model is spherical. All particles completely enclosed within the RVE are considered, as are all partially-enclosed particles. For the partially-enclosed particles, only the fraction of the particle within the RVE is considered in the calculation.

The initial intention of this model was to generate a packing that would fill up a spherical Representative Volume Element whose radius was unity. As the model's development progressed, however, it became clear that this would require an enormous number of particles (in excess of a thousand), and the rearrangement of this packing would take an excessively long time.

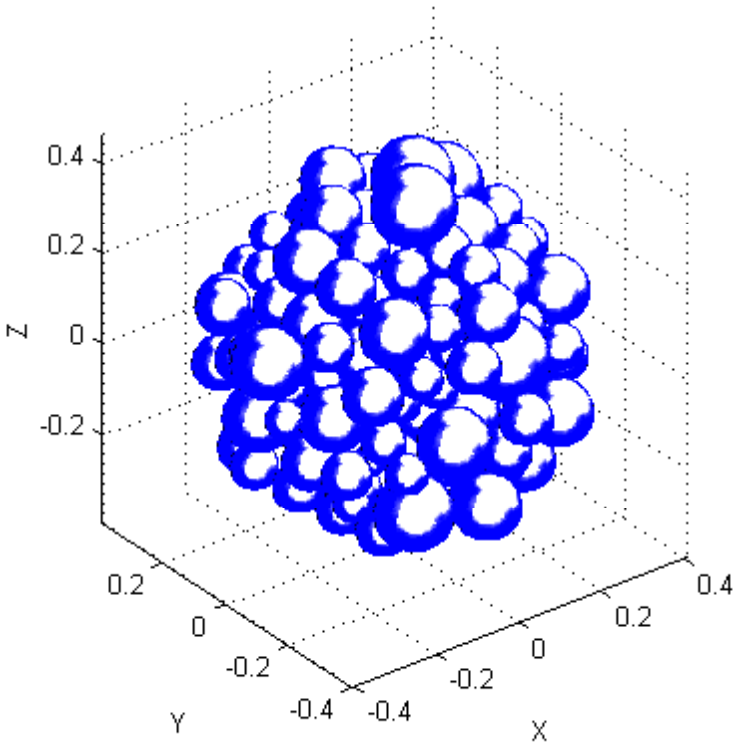

Figure 7. Selection of Representative Volume Element (RVE).

The model started with 300 particles. The RVE includes 221 particles, and has a radius of 0.3099.

4.3 Densification

The packing was "densified" by increasing the radii of all particles by the same percentage (generally in 0.5% increments), and computing the packing density, solid-solid surface area, solid-void surface area and mean coordination number. No rearrangement occurred after the "densification" process started.

The packing density is computed by determining, using Monte Carlo integration techniques, what fraction of the Representative Volume Element is occupied by particles. The solid-void surface area is computed for each particle, also using Monte Carlo integration

techniques, how much of its surface area is not inside other particles. The solid-solid surface area is computed by identifying the intersections between adjacent particles and computing their surface areas. The mean coordination number is computed by averaging the number of neighbors for each particle.

One feature of this model is that it treats sintering as a continuous process, rather than breaking it up into the stages described in Section 1.2. This eliminates some of the interpolations that would be needed if the model broke the sintering process up into stages.

4.4 Computer Software and Hardware

MATLAB® (for Matrix Laboratory) is a high-performance programming language and user environment for technical computing. It is particularly well-suited for computationally-intensive problems such as this one.

The core of the MATLAB® product is MATLAB® itself, including a program called Simulink, which simulates dynamic systems, and a number of optional extensions, called toolboxes. Some toolboxes are offered by The MathWorks®, the publisher of MATLAB®; others are written in MATLAB®'s programming language by other MATLAB® users. This application uses a toolbox called the Geometric Bounding Toolbox (GBT), which performs operations on polyhedra and ellipsoids. GBT is capable of defining and manipulating higher-order shapes, although this particular feature is not needed for this application. GBT was selected because it allows for mathematically compact definitions of complex shapes [30].

MATLAB® allows the model to be refined and extended easily. MATLAB®'s programming language is easy to learn, so future researchers will have little difficulty in working

with the model. The model created by Krishnan, which provided good results, was inflexible and could not be modified and refined as needed.

The student version of MATLAB® was used for this application (version 5.3). There are no fundamental differences between the student version of MATLAB® and the professional version; the student version of Simulink, which was not used for this model, has significant functional differences. The programming was done on a Gateway computer using a Pentium 4 CPU operating at 1.4 GHz, running Microsoft Windows Millennium Edition.

5.0 RESULTS

The results are shown on the following pages. The intermediate stage model and the data for the 0.17 μm and 0.4 μm alumina are taken from [6], and the Krishnan model data are taken from [25].

Figure 8 shows the relationship between packing density and densification. As explained in Section 4.3, densification is simulated by increasing the radii of all particles by the same percentage, in 0.5% increments. The origin of the plot, at which densification is zero, represents the initial packing.

Figure 9 shows the solid-void area versus packing density. This graph shows that S_V^{SV} decreases with increasing density; however, a slower rate of decrease is expected. In fact, the computed value of S_V^{SV} goes to zero at a packing density of about 93%, indicating a problem with the model in this area. This is discussed further in Section 6.0.

Figure 10 shows the relationship between the solid-solid surface area and the packing density. S_V^{SS} increases steadily with increasing density, then begins to level off at a packing density of about 95%.

Figure 11and Figure 12 show the model results for the intercept ratio Λ and the surface area ratio Ψ, respectively, and compare them to results from Krishnan's model and to experimental results. The current model shows little agreement with previous models and with experimental data, except at lower packing densities (below 70%). This is a result of the behavior of the solid-void surface area, as shown in Figure 9.

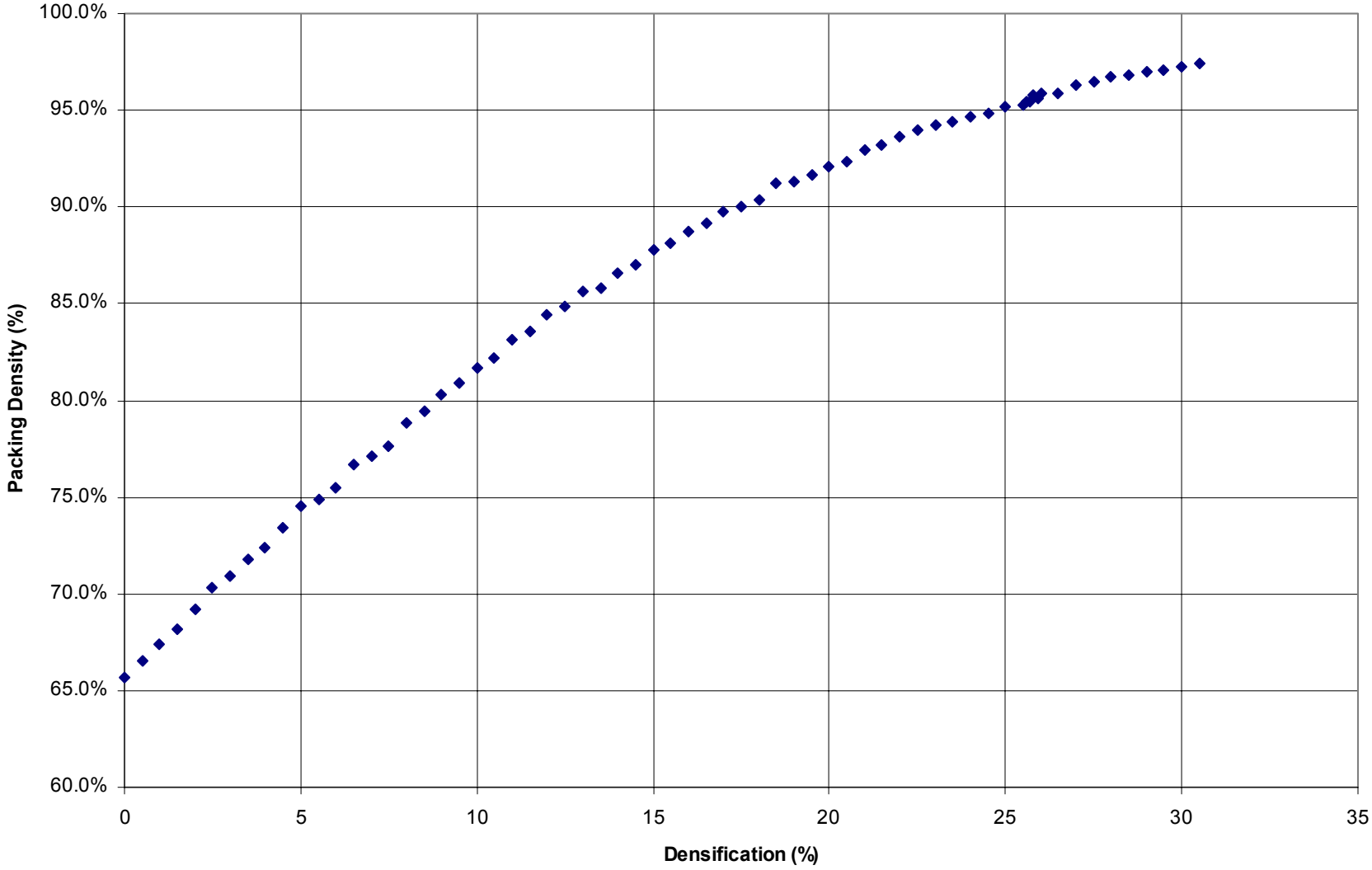

Figure 8. Packing Density versus Densification.

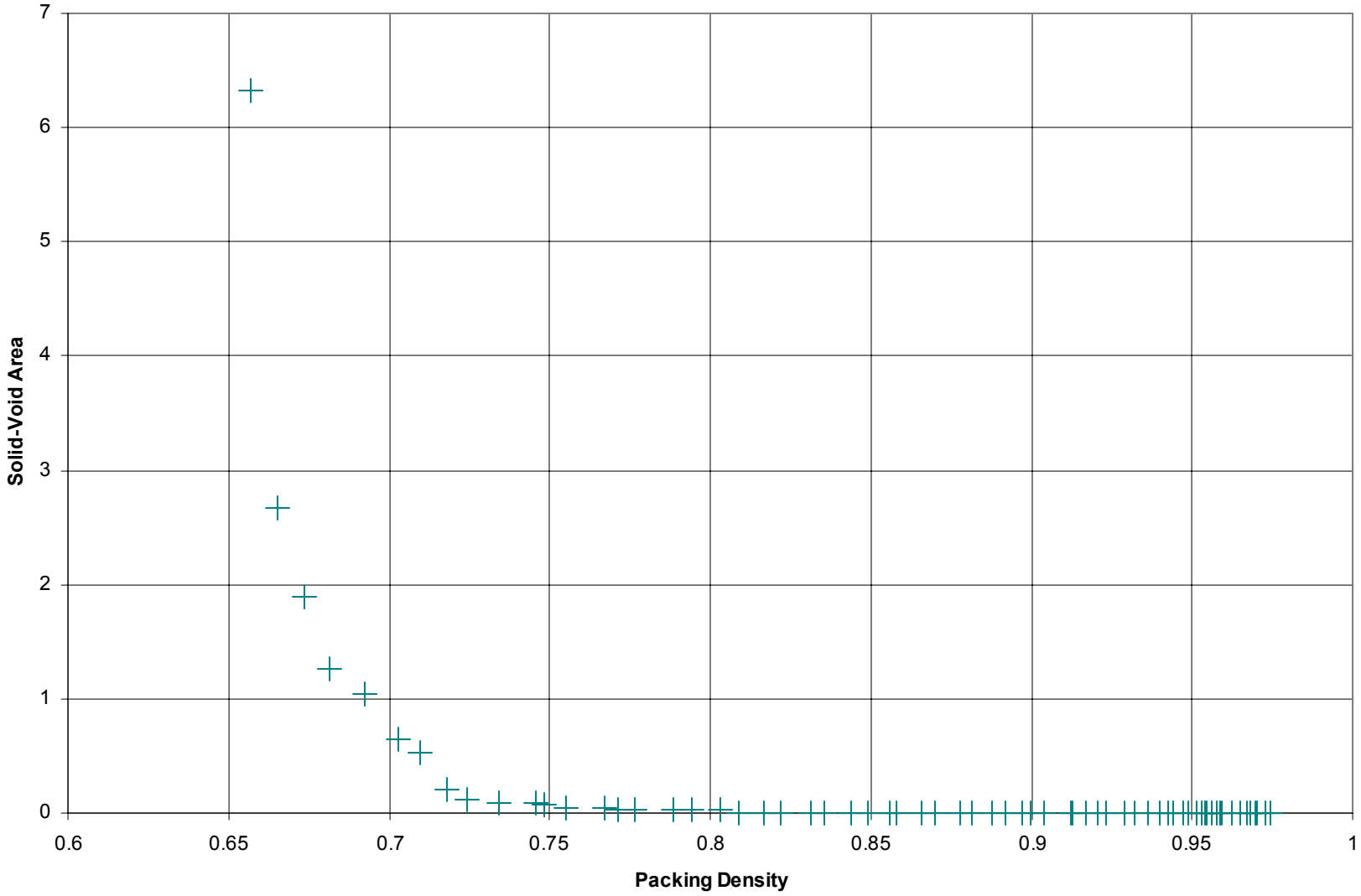

Figure 9. Solid-Void Surface Area versus Packing Density.

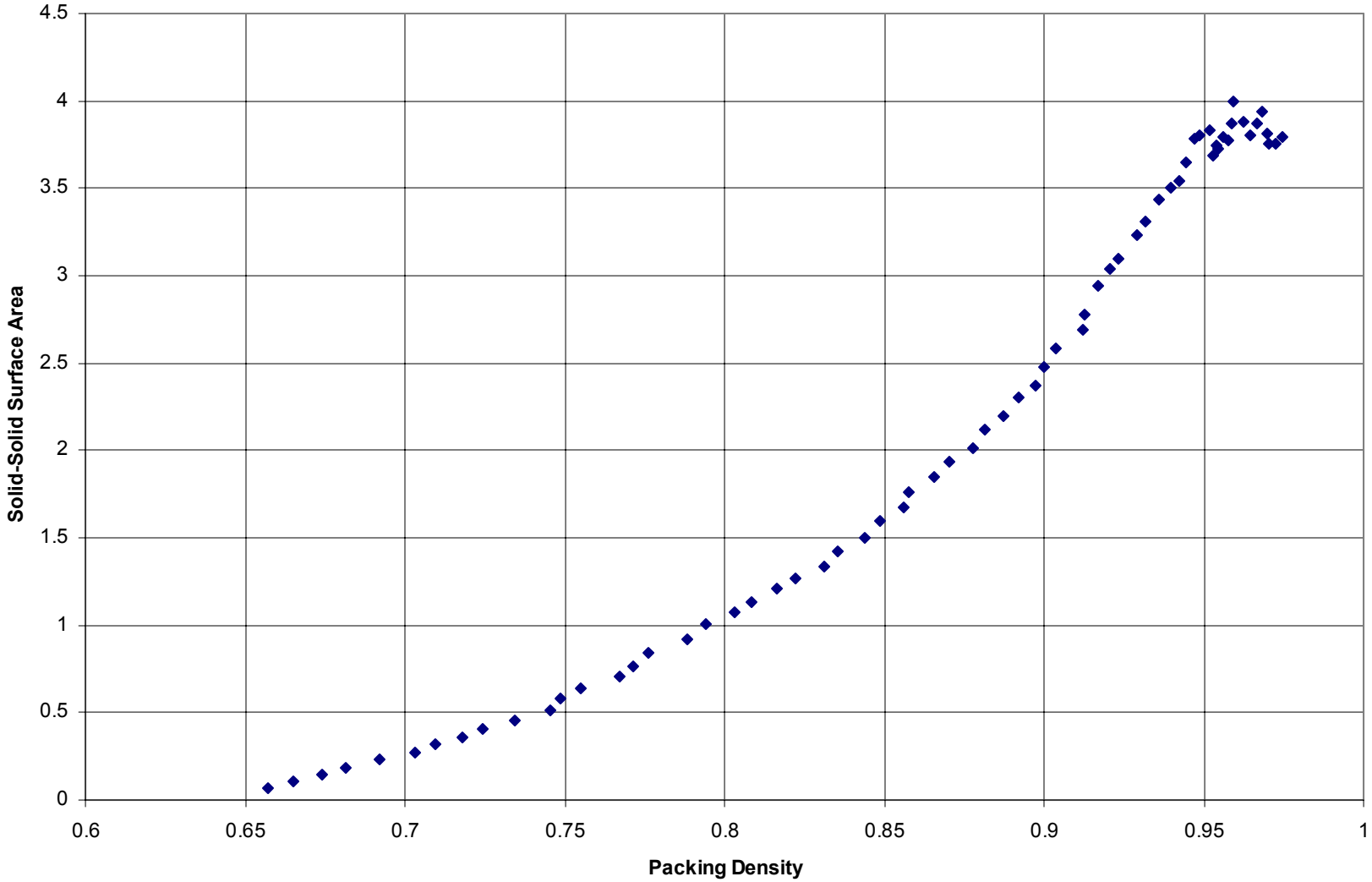

Figure 10. Solid-Solid Surface Area versus Packing Density.

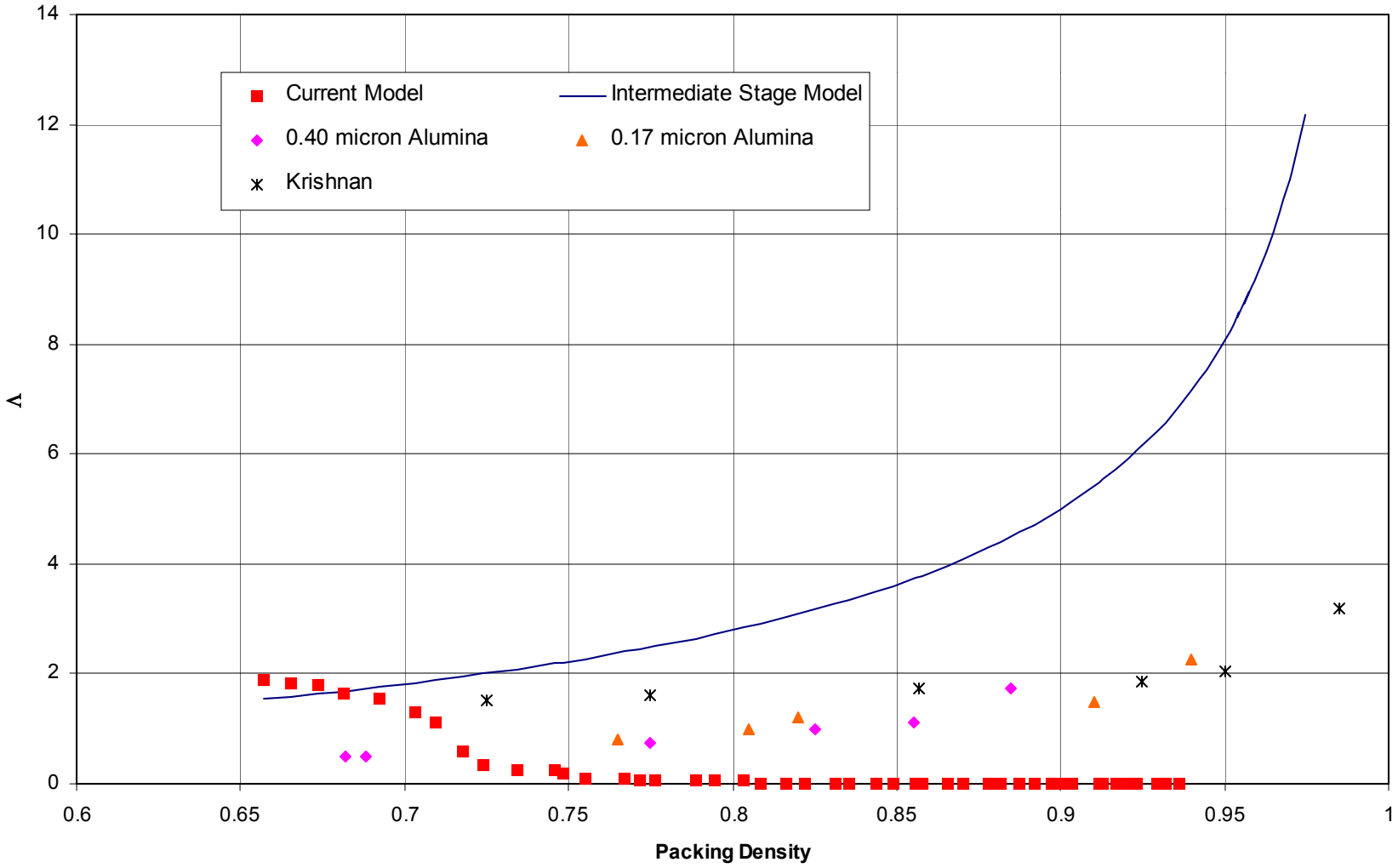

Figure 11. Intercept Ratio Λ versus Packing Density.

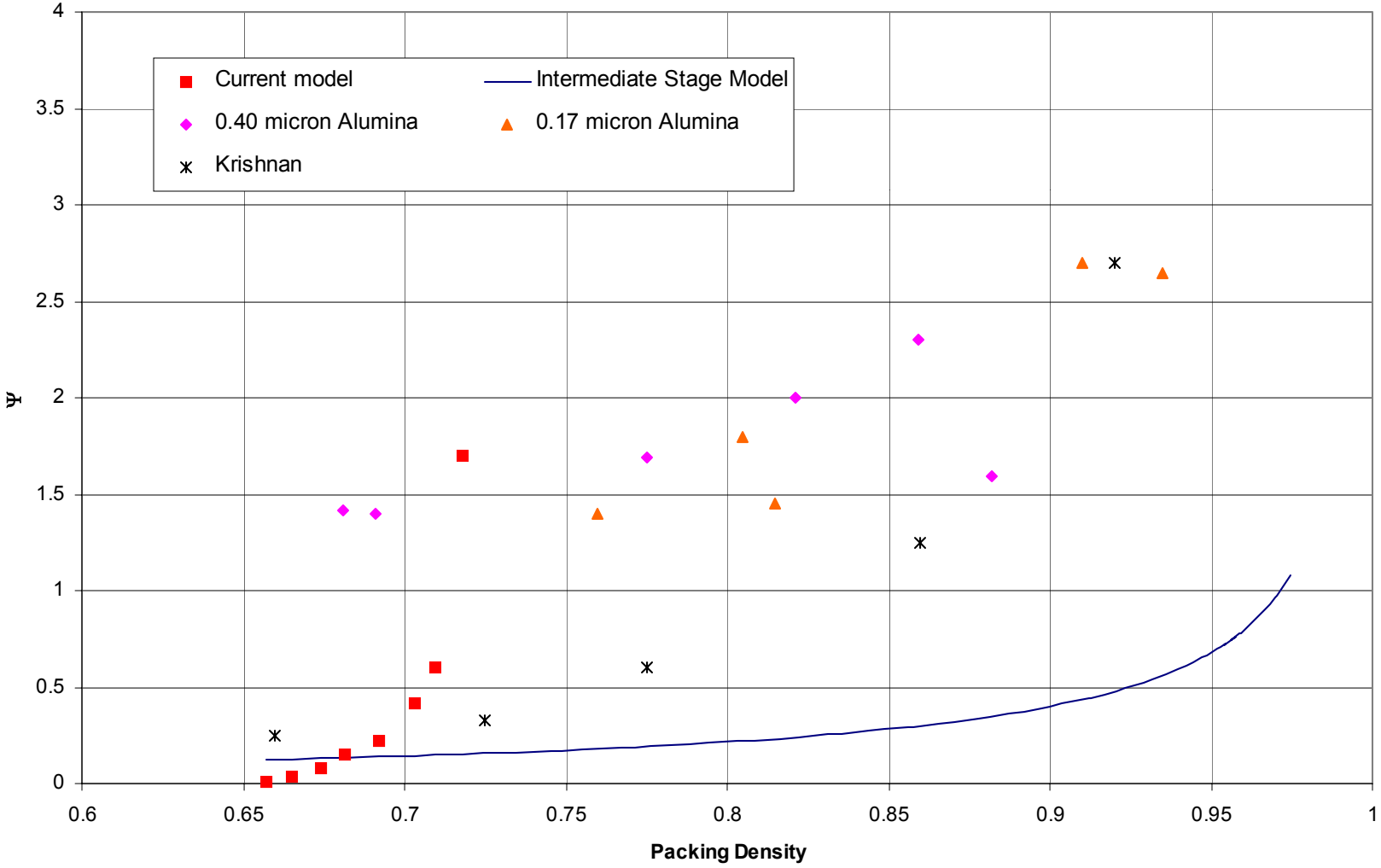

Figure 12. Surface Area Ratio Ψ versus Packing Density.

6.0 DISCUSSION

The current model shows poor agreement with previous models and with experimental data. This is largely due to problems with the solid-void surface area calculation.

As shown in Figure 9, the solid-void surface area falls off very rapidly, and reaches zero at a packing density of 93%. Logically, the solid-void surface area would be expected to decrease linearly, and reach zero at a packing density of 100%. An examination of the model suggests that the method used to compute the solid-void surface area may be at fault.

The solid-void surface area for each particle is computed as follows. A set of N data points is generated at random on the surface of the particle. Each point is defined in terms of its spherical coordinates local to the particle (R, φ, θ) and has an incremental area unit dA associated with it. The number of points is proportional to the square of the radius; in this case, $10{,}000R^2$ points are generated on each particle. Each data point is examined against the particle's neighbors. If the data point is not located inside any of the neighboring particles, it forms part of the solid-void surface. If this is the case, the value of counter j is incremented by sin θ. Sin θ is used (instead of unity) to ensure that particles at the poles (where sin θ = 0) are not weighted more heavily than particles at the equator (where sin θ = 1).

Once all data points have been examined, the solid-void surface area for the particle is calculated:

$$SV_i = 2\pi^2 R_i^{\,2} \frac{j}{N_i}$$

Where R_i is the radius of the i^{th} particle, and N_i is the total number of data points examined. The quantities SV_i are stored in an array. Once all particles have been considered, the total solid-void surface area is computed by summing all the values of SV_i.

Monte Carlo integration is a technique that requires an exceptionally large number of data points to converge. It is possible that $10{,}000R^2$ data points on the surface of each particle is insufficient. However, a few trial runs with larger numbers of data points indicate that this is not the case. In these trials, using 10,000 data points yielded results that were different by less than 10%. Furthermore, using more data points did not, in general, increase the calculated solid-void surface area; at some densities, the solid-void surface area calculated with more data points was actually lower.

This fact leads to the conclusion that Monte Carlo integration is not a suitable method for computing the solid-void surface area, at least for the packing under investigation. A purely geometric method may need to be employed. This would involve checking the intersection between the particle under consideration and each of its neighbors, computing the distance between centers, computing the area of the spherical cap created by the intersection, and subtracting that surface area from the total surface area of the particle.

The solid-solid surface area increases almost linearly with packing density, and then begins to level off at a packing density of around 95%. This reduction results from the fact that, as smaller particles are absorbed by larger ones, the solid-solid surface area computed by the algorithm is actually smaller than the surface area of the plane through the smaller particle's center. See Figure 13. At a packing density of 95%, none of the particles has been completely

absorbed by any others. Physically, this is analogous to grain growth, which occurs during final stage sintering.

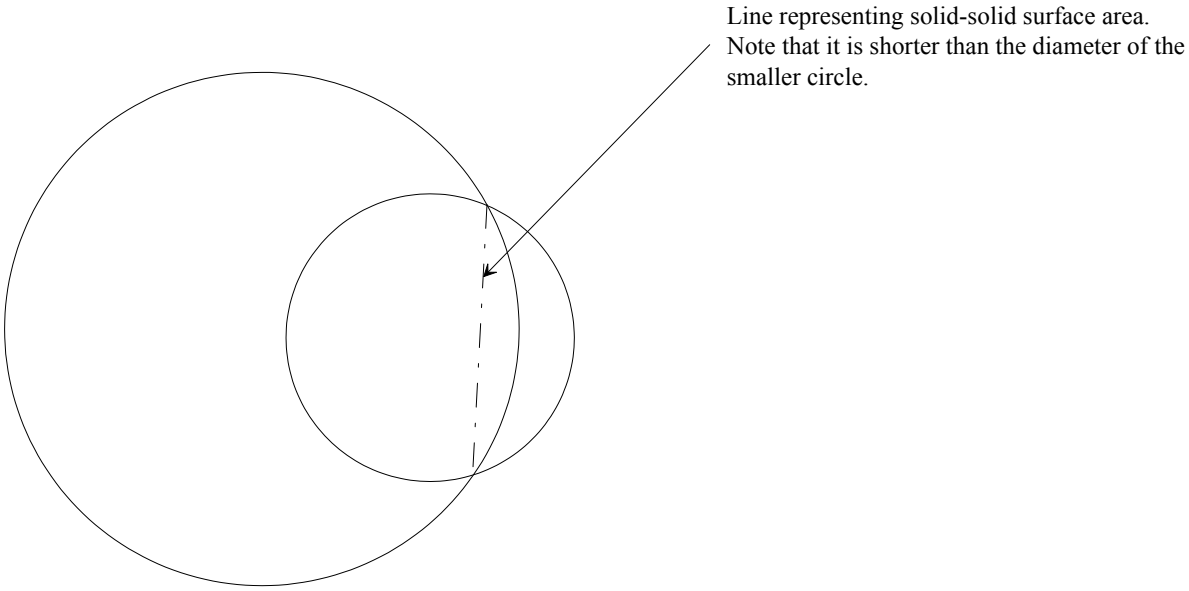

Figure 13. Solid-Solid Surface Area Between Two Particles.

7.0 CONCLUSIONS

The results from this simulation are disappointing. The problems with the model are described in the previous section. However, the model presents some positive features. It generates a close packing, and can be extended to model other sintering conditions.

Once the problems with the calculation of the solid-void surface area have been addressed, this model may prove valuable in predicting the microstructural properties of a sintered part based on its geometric properties.

8.0 DIRECTIONS FOR FUTURE RESEARCH

The model created for this thesis has many advantages. MATLAB® is a powerful and easy to use programming language, with many built-in functions and a great deal of flexibility. Modifying and extending the model is therefore simplified.

Improvements to the model can be made in several areas. First, as noted in Section 6.0, the method for computing the solid-void surface area needs to be improved. A possible solution to this problem is outlined in Section 6.0. The particle packing model can also be improved, as discussed in Section 8.1 below. Finally, different sintering conditions (pressure assisted sintering, particle movement during sintering, etc.) can be added to the model, as discussed in Section 8.2 below.

8.1 Refining the Particle Packing Model

Some problems with the particle packing model were identified during its development. Some difficulty was experienced in getting a close-packed compact when rearranging the particles. It is believed that a combination of the following modifications may facilitate getting a close packing:

- Modifying the initial distribution of particle centers,
- Refining the rearrangement geometry (particle movement during rearrangement).

Increasing the number of particles may also assist in getting a close packing. This was attempted only on a limited basis, as the particle rearrangement algorithm required a lot of computer time.

The current model also fails to take any account of the pore size distribution, which may play a significant role in the evolution of the microstructure. Zheng and Reed [23] found that there is a critical ratio of pore size to mean particle size. Pores smaller than this critical ratio were completely eliminated during sintering, while pores larger than the critical ratio were not. This is an area that was not explored in the course of this research; however, algorithms for measuring pore size and pore size distribution exist [31].

8.2 Simulating Different Sintering Conditions

Once a close packing has been achieved, refinements can be made to the densification part of the model. For instance, a real compact experiences some particle movement during sintering. This could be integrated into the rearrangement algorithm, by allowing particle rearrangement between densification steps. Pressure sintering (hydrostatic or isostatic) could also be simulated. This could be done by allowing particle rearrangement between densification steps, and imposing a preferred direction of movement, either towards the center of the packing (for hydrostatic pressure) or downwards (for isostatic pressure). These refinements would improve the model's ability to predict microstructural pathways during sintering, and eventually to help predict the finished shape of a sintered product.

APPENDIX A

SIMULATION CODE DESCRIPTION AND ALGORITHMS

The code for the simulation was based on a particle packing routine described by Nolan and Kavanagh [11, 26]. The algorithms for their routine, which was originally written in Pascal, were modified and rewritten in MATLAB® for this application.

The simulation proceeds in three stages. In the first stage, an initial packing is generated, and certain parameters (nearest neighbors, packing density, overlap, etc.) are computed and stored. The second stage consists of rearranging the packing to minimize overlap and maximize stability. The third stage consists of expanding (densifying) the packing and computing its geometric and stereological properties.

Following are verbal descriptions of each section of the code. For sections for which a verbal description is insufficient, a flowchart showing the algorithm is provided.

Generating the Initial Packing

Generate

This routine generates a random packing of spherical particles. There are NumSpheres particles, each with a center c and radius r. The particle definitions are stored in a 4 x NumSpheres array called Particle. Each row of Particle is structured as [x y z r], where x, y and z are the Cartesian coordinates of the center of the particle, and r is the radius. The spheres are generated within a unit sphere. A sphere is used (instead of some other shape) because it avoids edge effects, and because it is isotropic. NumSpheres is entered by the user.

The particles are initially generated around the origin of the unit sphere (that is, particle centers are normally distributed with $(\bar{x}, \bar{y}, \bar{z}) = \hat{0}$), instead of uniformly throughout the unit

sphere. This allows a high initial degree of overlap and contact among the particles, which allows the packing to be rearranged more effectively. See "Rearranging the Particles" below.

Reduce

The initial packing created by generate places particles randomly in space. Some particles will be completely inside other particles, and some will be outside the unit sphere selected as the volume in which the packing is generated. This routine eliminates particles that are completely inside other particles and particles lying completely outside the unit sphere.

Findlocal

This routine computes an array called touch. The touch array is structured as follows. Each row represents one particle from the Particle array (i.e., the first row represents the first particle, the second row represents the second particle, etc.) The number in the first column indicates how many particles are in contact with that particle. For instance, the number "8" in the third row indicates that there are eight particles in contact with the third particle in the Particle array. The numbers in the 2^{nd} through n^{th} columns are the numbers of the contacting particles. In this example, the third particle is in contact with eight other particles: the first, fourth, sixth, 10^{th}, 17^{th}, 22^{nd}, 37^{th}, and 62^{nd}. See Figure 14.

The Findlocal routine finds up to 12 particles within one-half the mean particle radius of each particle.

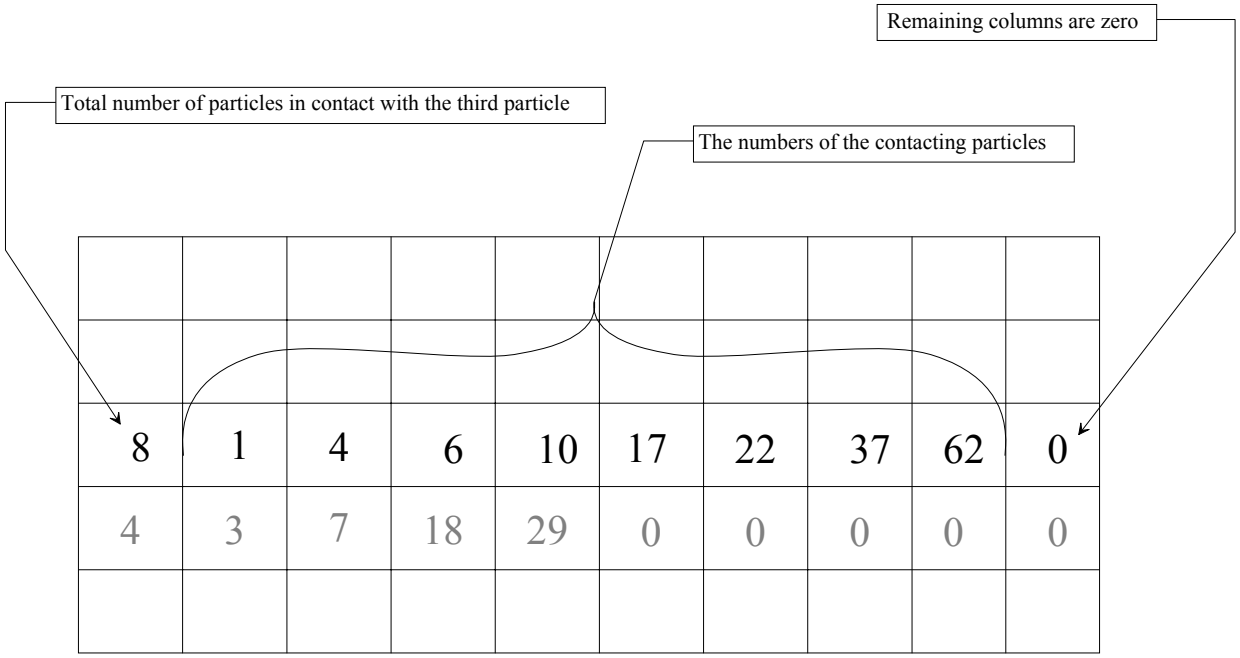

Figure 14. Layout of the touch Array.

Density

The Density routine computes the packing density of the particles, as described in Appendix C. The algorithm for this routine is shown in Figure 21.

Packstat

Packstat computes the packing statistics for the particle arrangement. These statistics include the separation and/or degree of overlap between adjacent particles, the mean coordination number of the arrangement, and the fraction of particles that are in a gravitationally stable configuration. A particle is gravitationally stable if it is supported from underneath by three other particles.

Rearranging the Particles

The packing generated above is not close-packed. The particles are placed in space at random; many of them overlap, while some are not in contact with any other particles. The purpose of the rearrangement is to shift the particles around to minimize overlap and maximize stability. The Rearrange routine loops as long as the mean overlap is more than one-sixth the mean particle radius, and the fraction of particles in a gravitationally stable configuration is less than 75%. The algorithm for this routine is given in Figure 19.

Subregion

After the packing is rearranged, most of the particles are clustered around the origin, as shown in Figure 15. This produces a very low packing density within the unit sphere, as most of the space in the unit sphere is empty. Therefore, a representative volume, or subregion, of the original packing is selected. This new subregion has a radius, RegionRadius, equal to the mean of the particle radii. Most of the particles are located in this subregion. The packing parameters and touch array are recomputed for the subregion. From this point, only the subregion is considered. This process eliminates the need to fill a large volume with particles, which would significantly increase computation time.

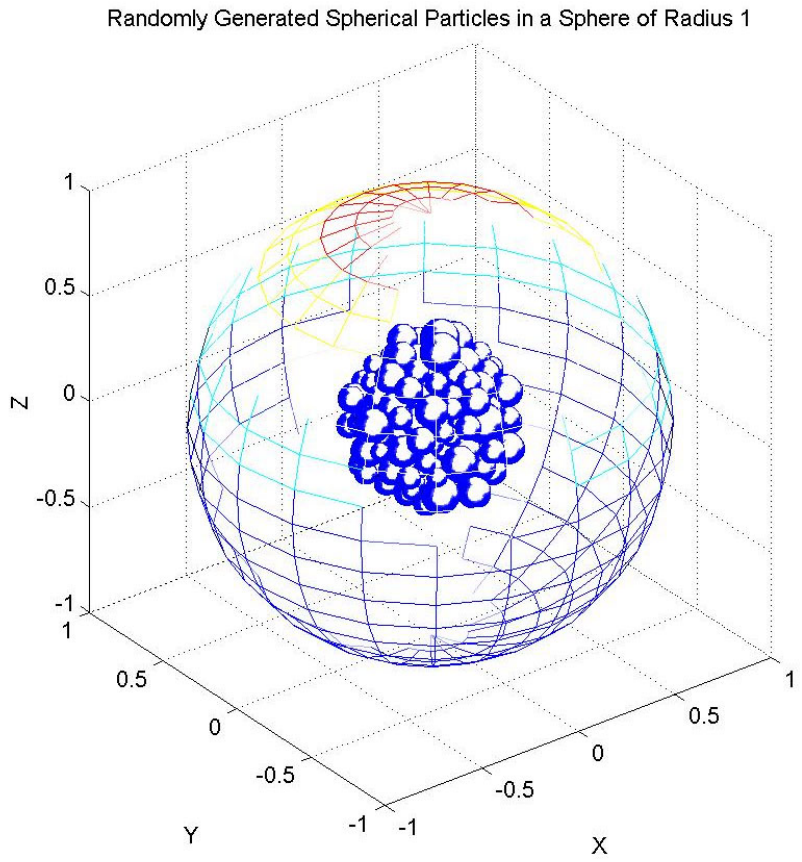

Figure 15. Location of Particles after Rearrangement.

Solidsolid

The solid-solid surface area between two overlapping spheres is a circle, as shown in Figure 16. The area of this circle, whose radius is a, is given by πa^2, where $a = \frac{1}{2d}\sqrt{4d^2R^2 - (d^2 - r^2 + R^2)^2}$, R and r are the radii of the larger and smaller spheres, respectively, and d is the distance between the particle centers.

Figure 16. Intersection Between Two Spheres.

The situation is more complex when more than two spheres overlap at a point in space. Physically, this is roughly equivalent to the point at which the necks begin to impinge on each other. The problem can be illustrated in two dimensions with three overlapping circles. See Figure 17.

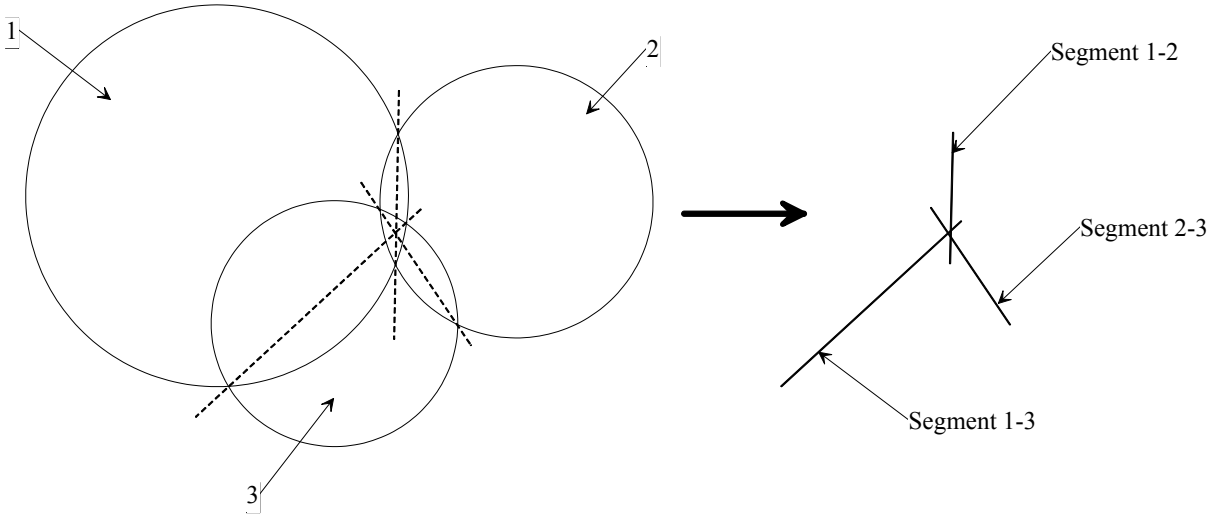

Figure 17. Intersection of Three Circles.

To compute the total contact length among circles 1, 2 and 3 (analogous to the total contact area among three spheres), one needs to consider parts of line segments 1-2, 1-3 and 2-3:

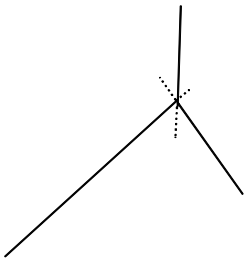

Figure 18. Total Contact Length for Three Circles.

The dotted line segments in Figure 18 must be removed from the calculation. While this is simple enough in this example, it becomes very complicated in three dimensions, especially with more than three particles.

The Geometric Bounding Toolbox (GBT), mentioned elsewhere in this thesis, includes a routine that computes the contact area of multiple contacting spheres in space. Results from this routine were compared with results computed geometrically from 2- and 3-particle systems, which are relatively simple to compute geometrically. The results returned by the GBT were within 1% of the geometrically calculated results.

Solidvoid

This routine computes the solid-void surface area of the packing, as described in Appendix C. The algorithm for the solid-void calculation is given in Figure 27 and Figure .

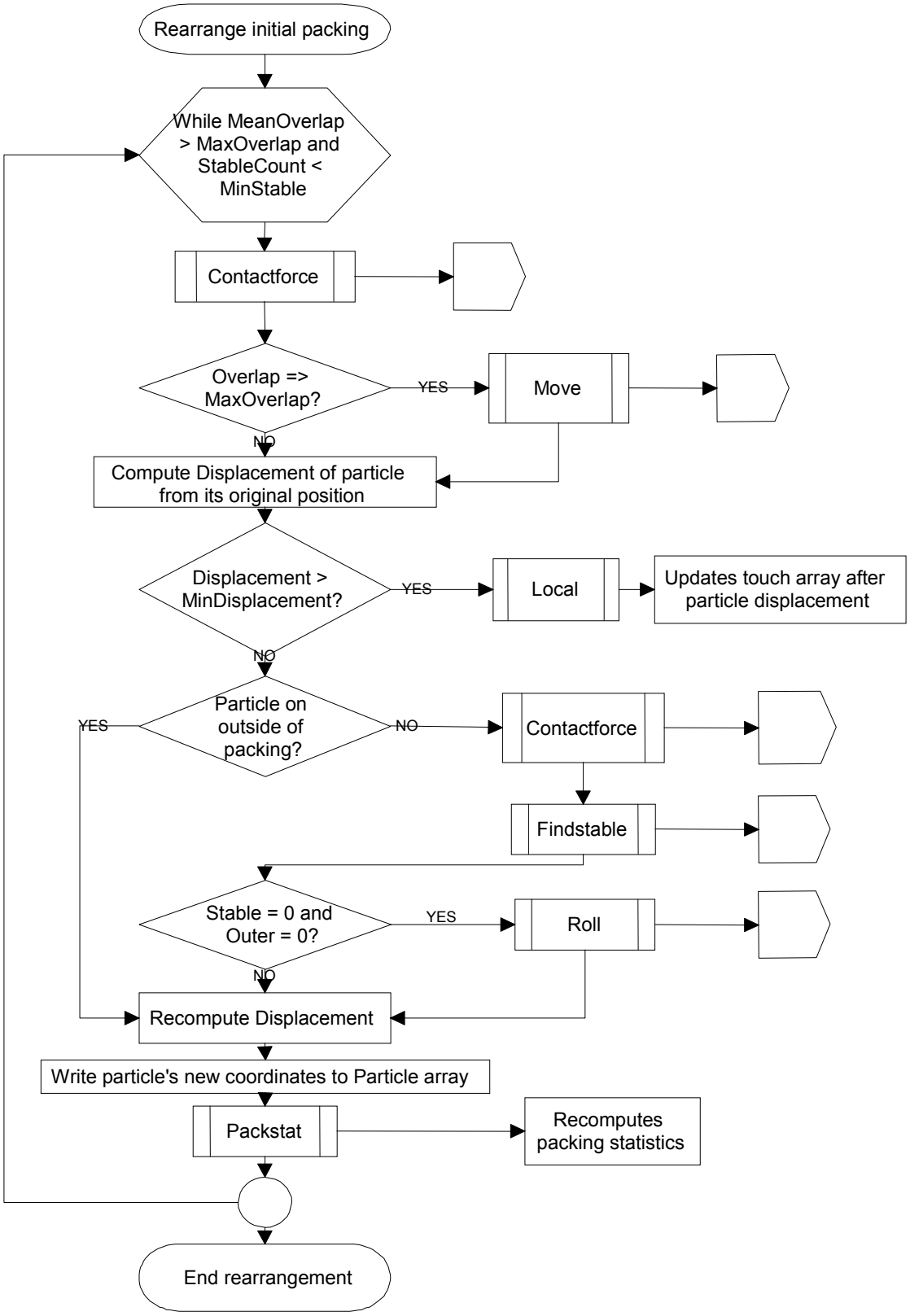

Figure 19. Algorithm for Rearrange.

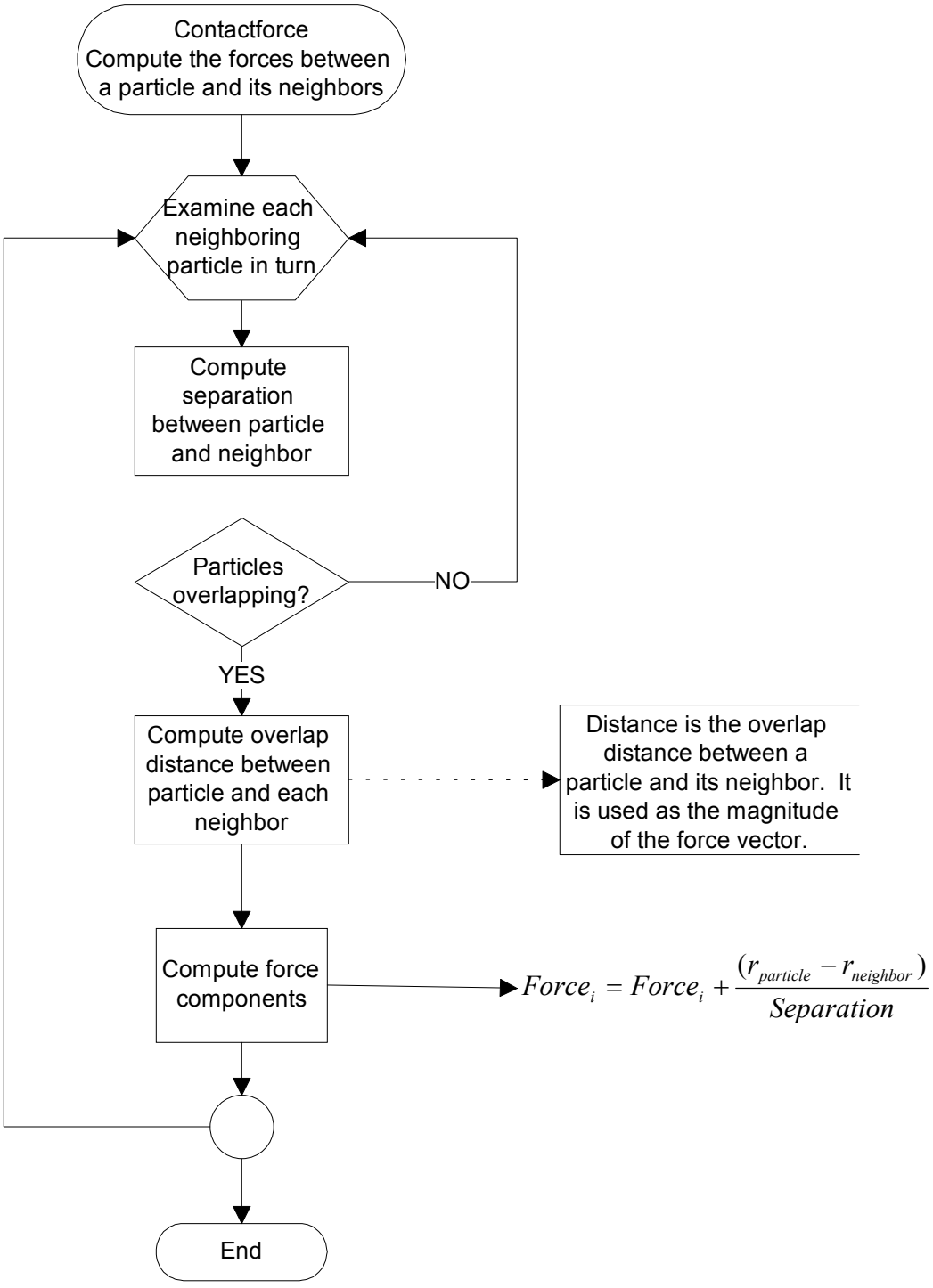

Figure 20. Algorithm for Contactforce.

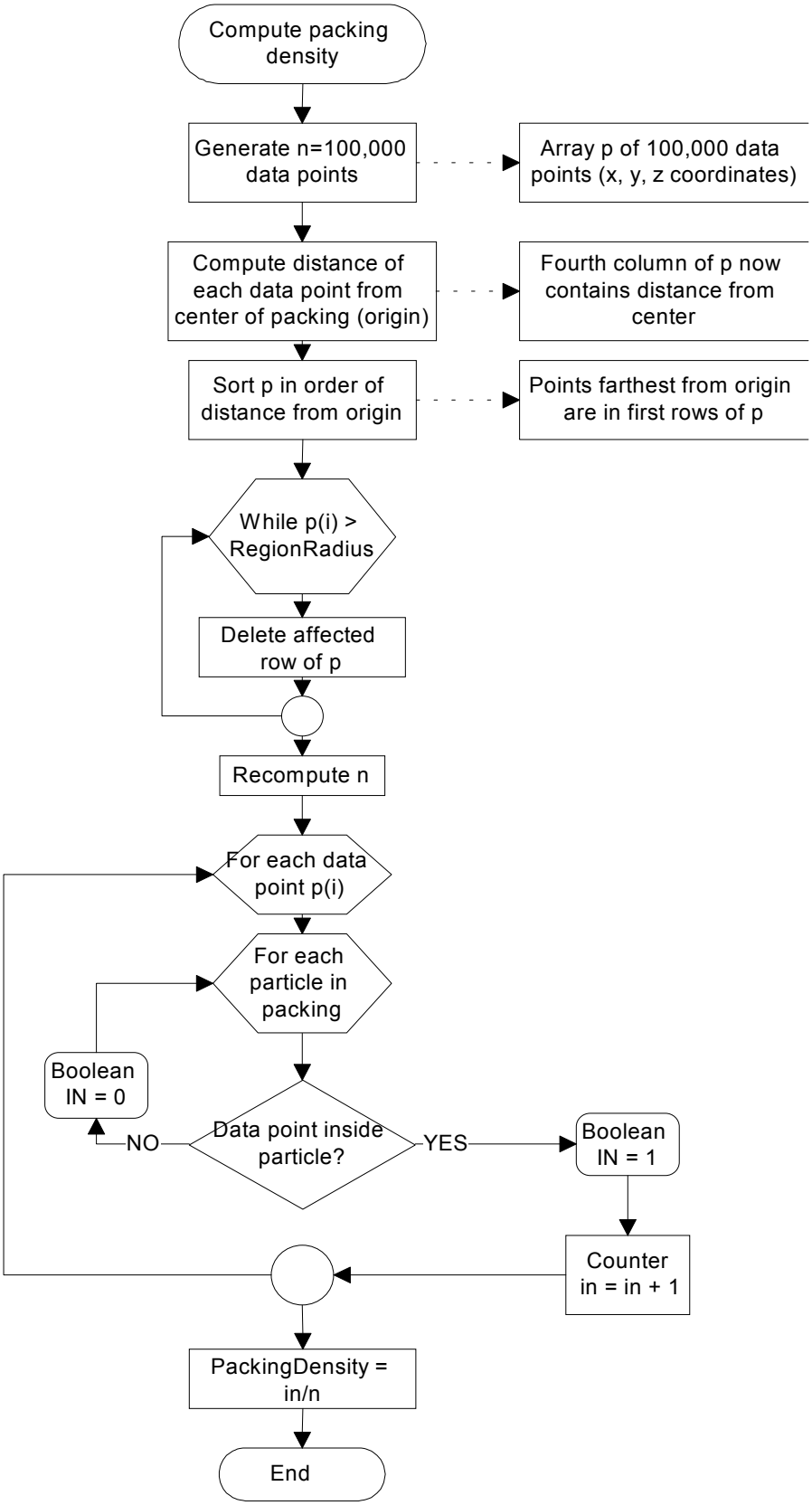

Figure 21. Algorithm for Density.

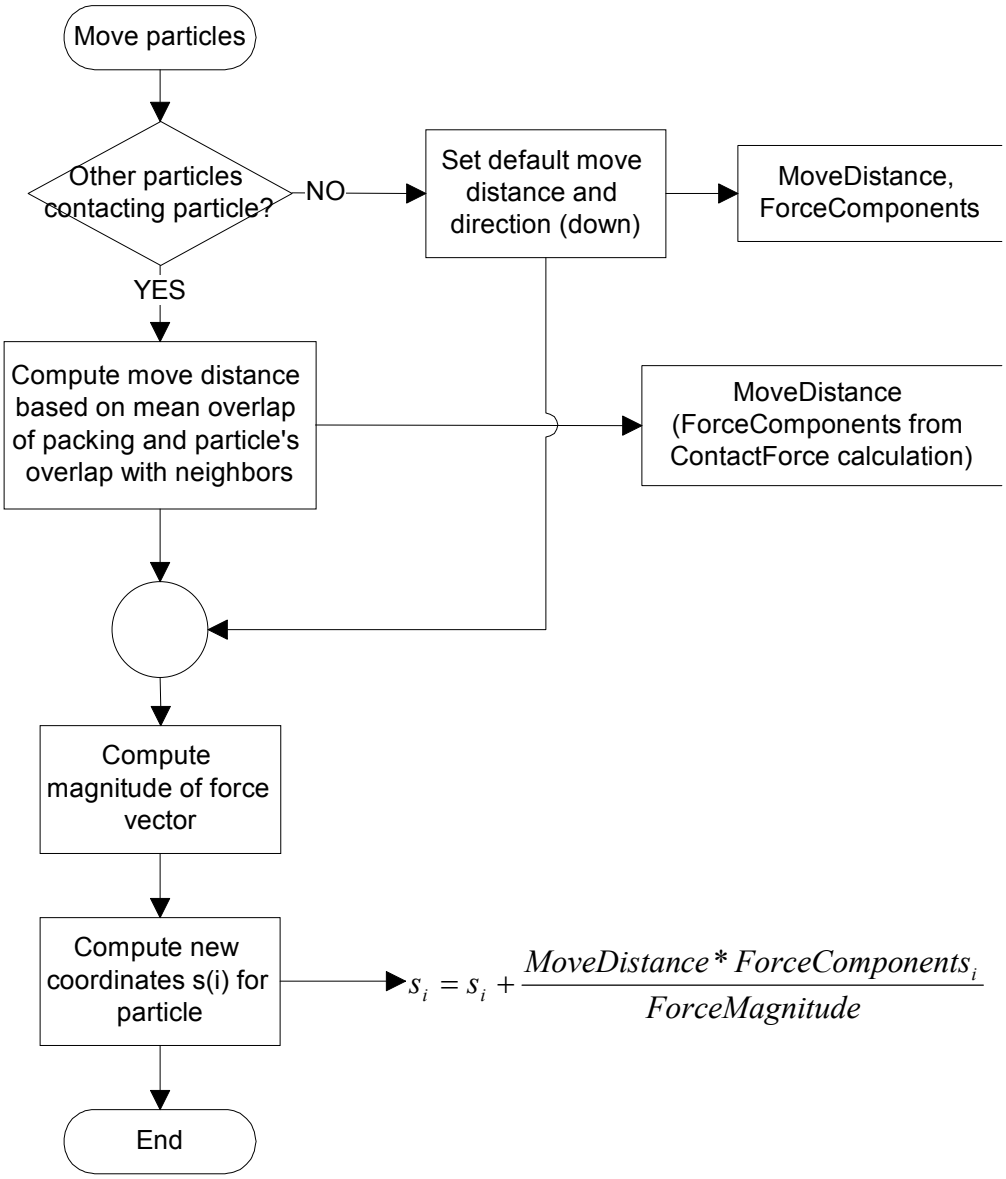

Figure 22. Algorithm for Move.

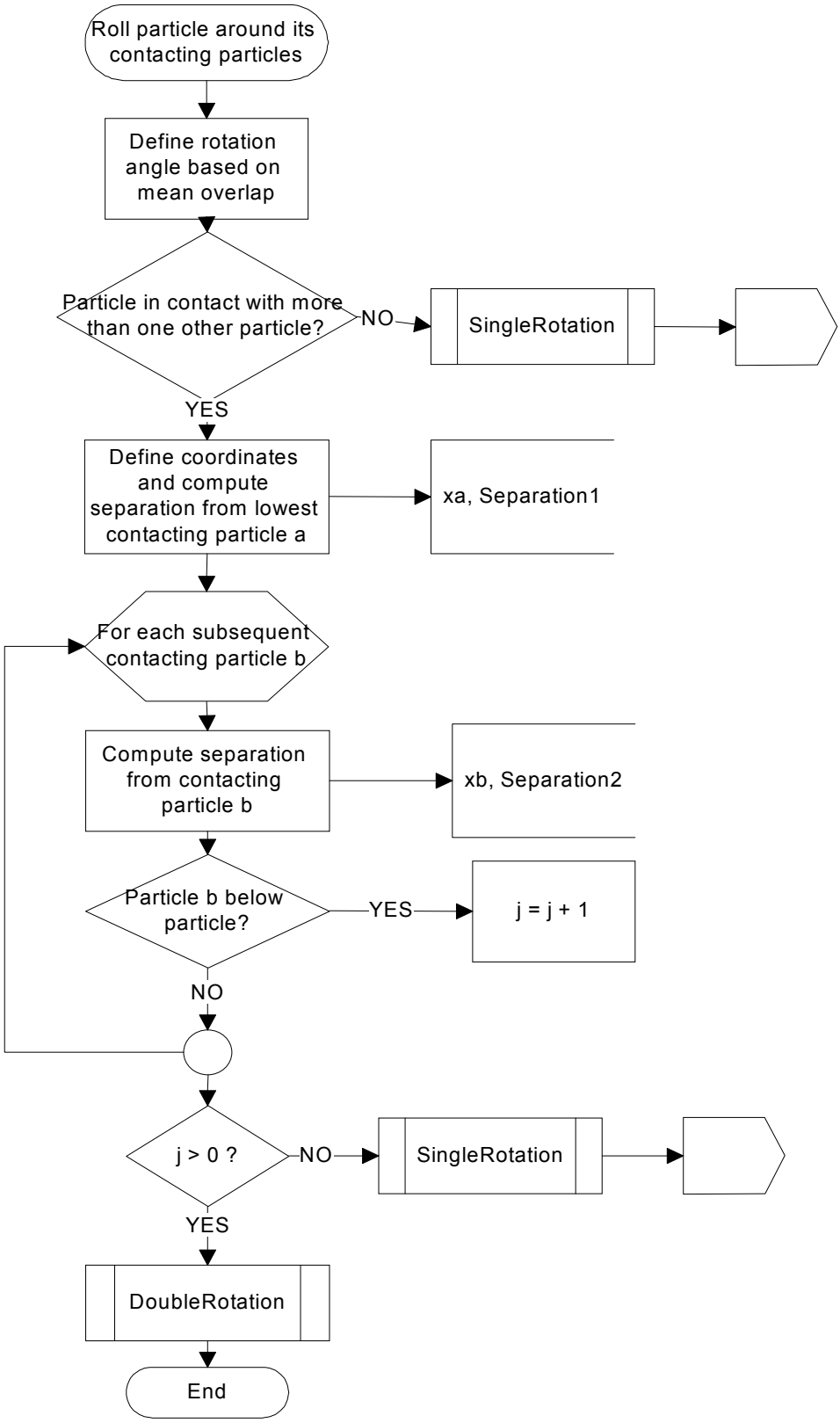

Figure 23. Algorithm for Roll.

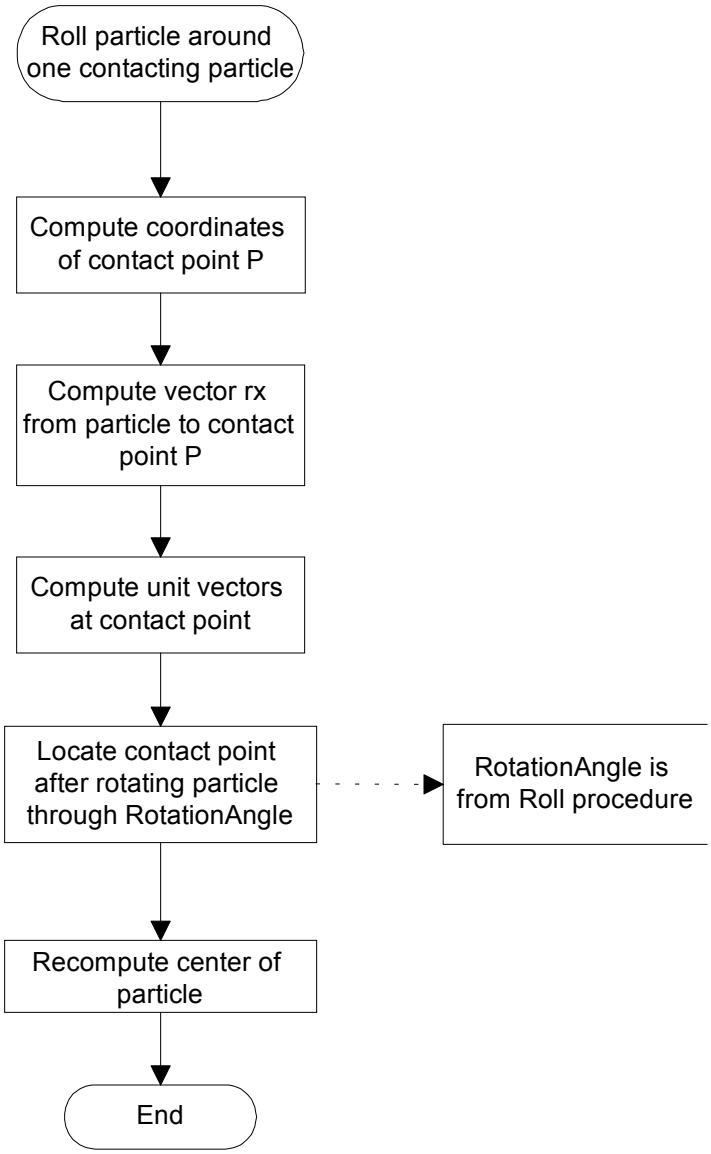

Figure 24. Algorithm for SingleRotation.

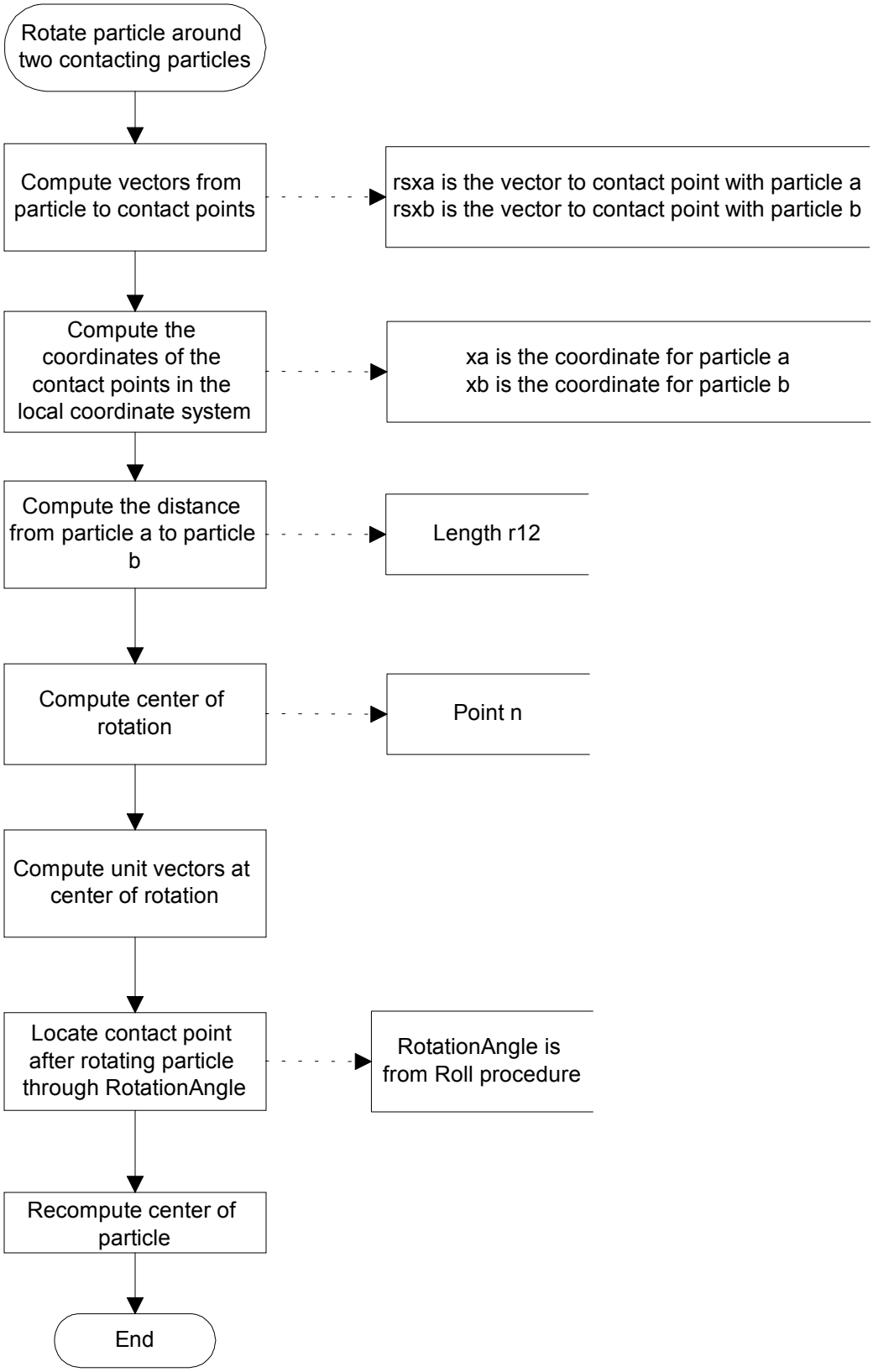

Figure 25. Algorithm for DoubleRotation.

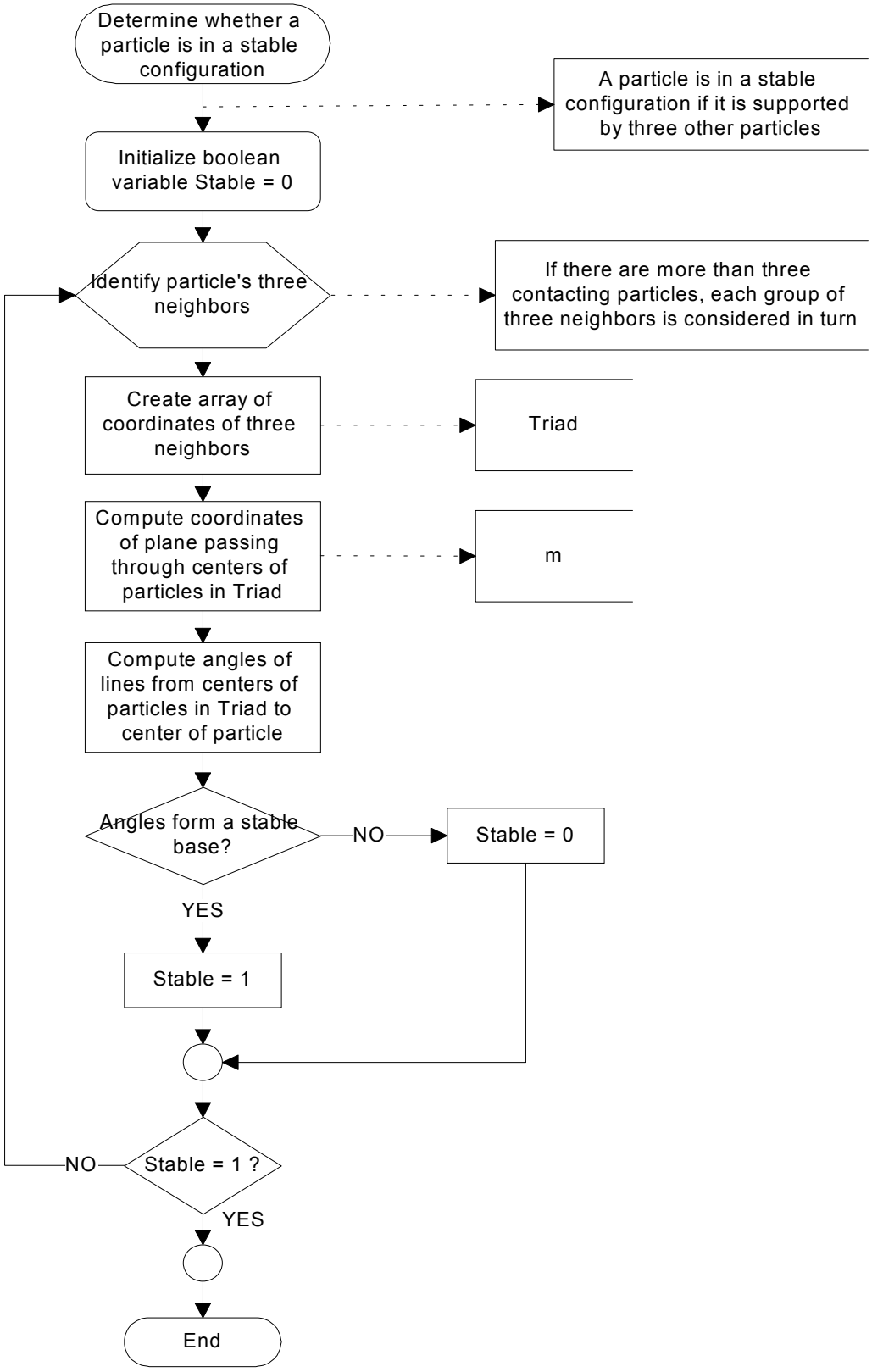

Figure 26. Algorithm for Findstable.

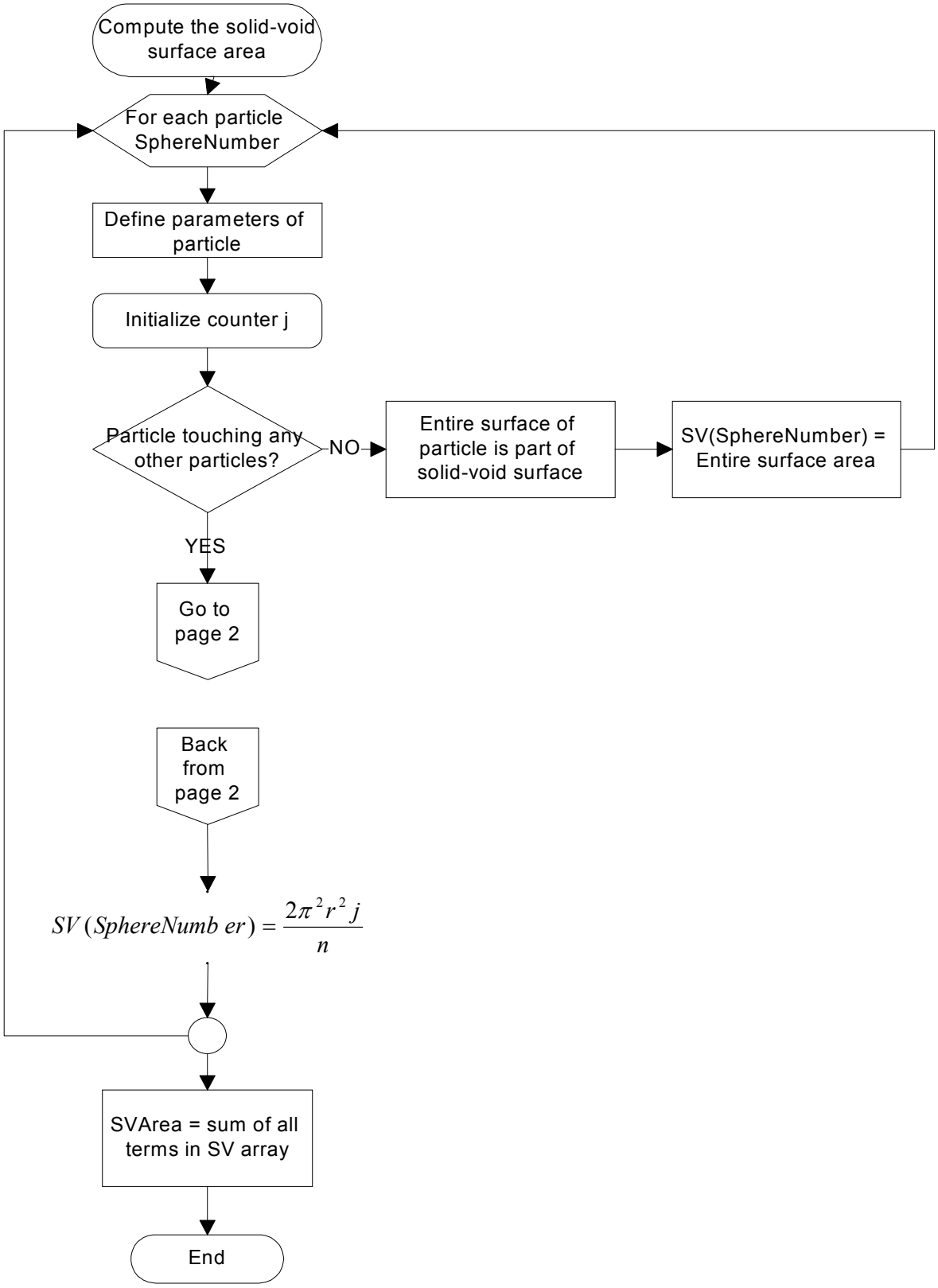

Figure 27. Algorithm for Solid-Void Calculation.

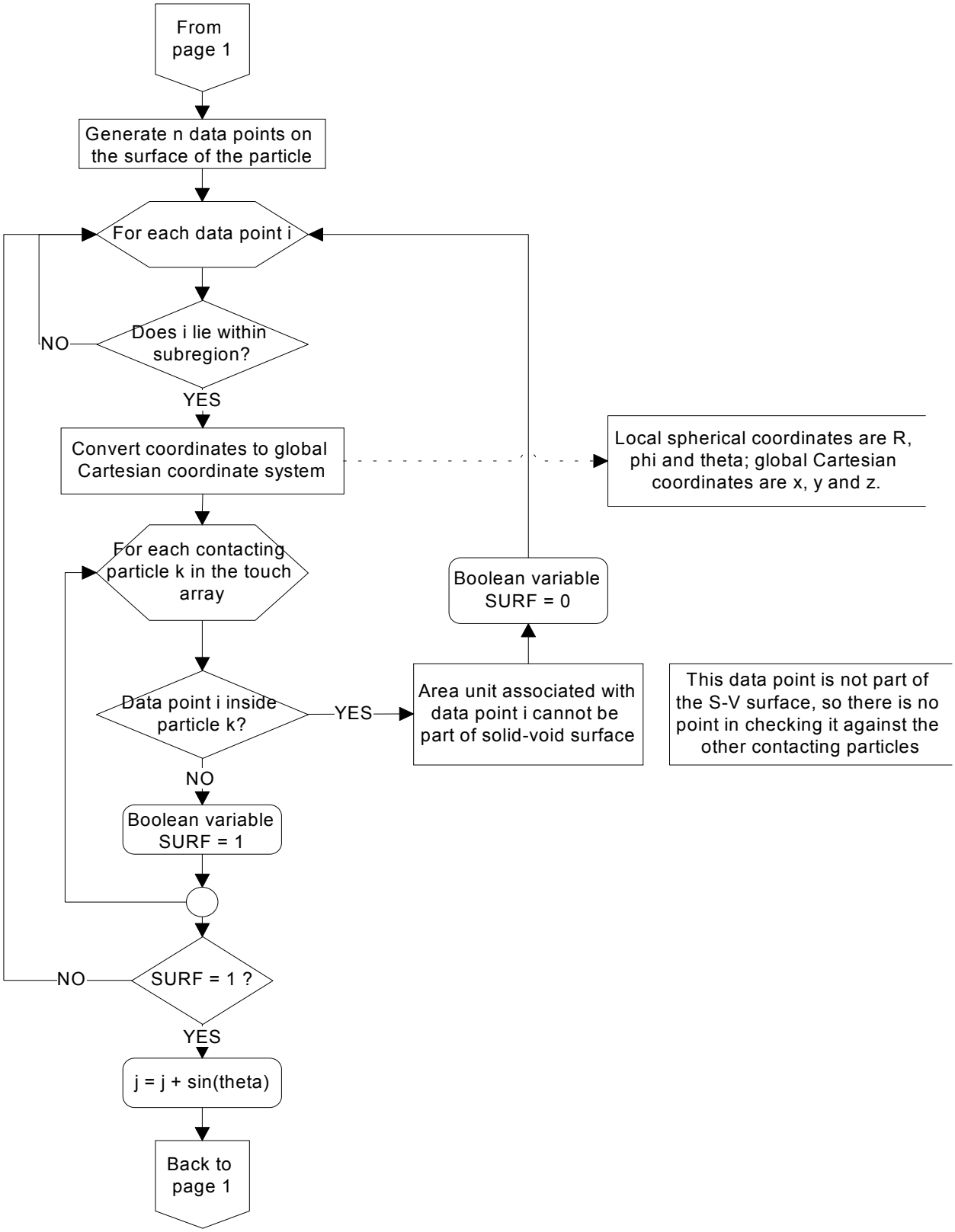

Figure 27 (continued). Algorithm for Solid-Void Calculation.

APPENDIX B

THE LOG-NORMAL DISTRIBUTION

Many researchers consider that the log-normal distribution best represents the true particle size distribution [12, 13]. The log-normal distribution is a continuous distribution in which the logarithm of a variable x is normally distributed [22]. It is described by

$$P(x) = \frac{1}{x\sigma\sqrt{2\pi}} e^{\frac{-(\ln(x)-\mu)^2}{2\sigma^2}}$$

Where μ is the mean of the underlying normal distribution, and σ^2 is the variance of the underlying normal distribution. The mean and variance of the log-normal distribution are given by

$$\mu_{\ln} = e^{\mu+\sigma^2/2}$$

and

$$\sigma_{\ln} = e^{\sigma^2+2\mu}(e^{\sigma^2}-1)$$

An example of the log-normal distribution is shown in Figure 28.

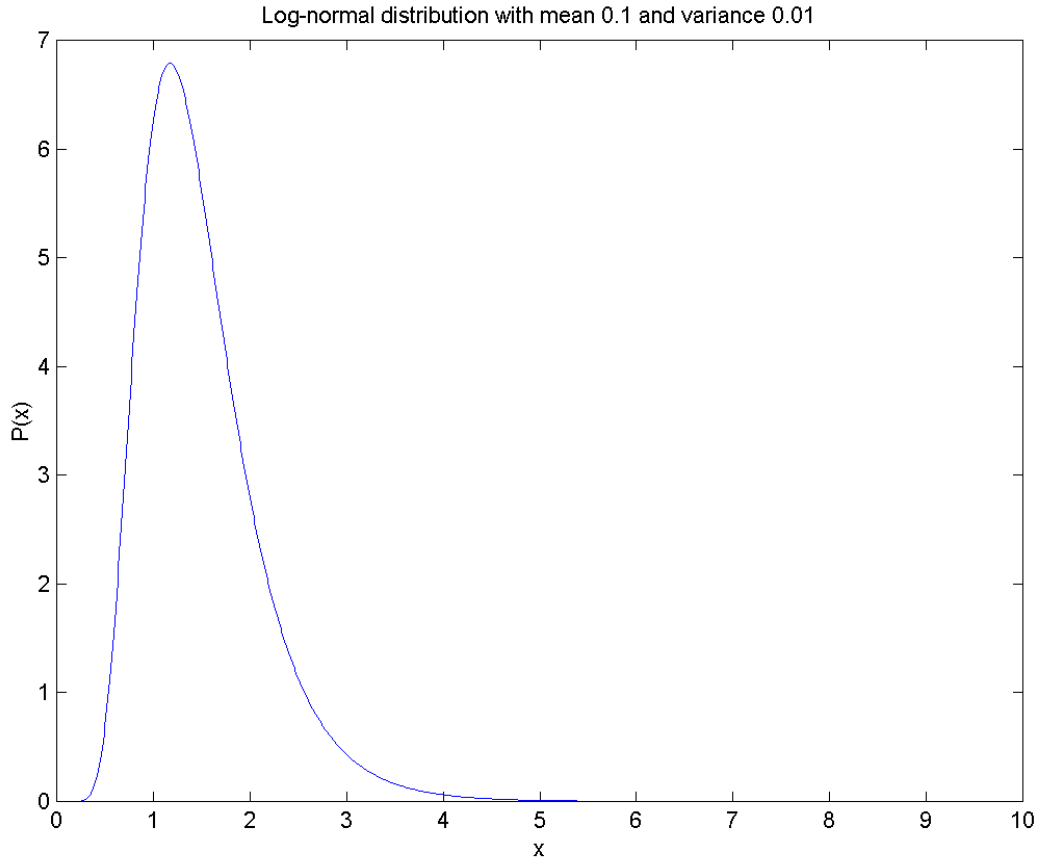

Figure 28. The Log-Normal Distribution.

The log-normal distribution is skewed to the left relative to a normal distribution with the same underlying mean and variance.

APPENDIX C

MONTE CARLO INTEGRATION

C-1 Background

Monte Carlo integration is a numerical integration technique that can be used to estimate the value of an integral when an analytical solution cannot be found [32]. Consider the integral $I = \int_a^b g(x)dx$ as representing the area under the curve g(x) from a to b as shown in Figure 29. Ω denotes the rectangle defined by a, b and c, as shown.

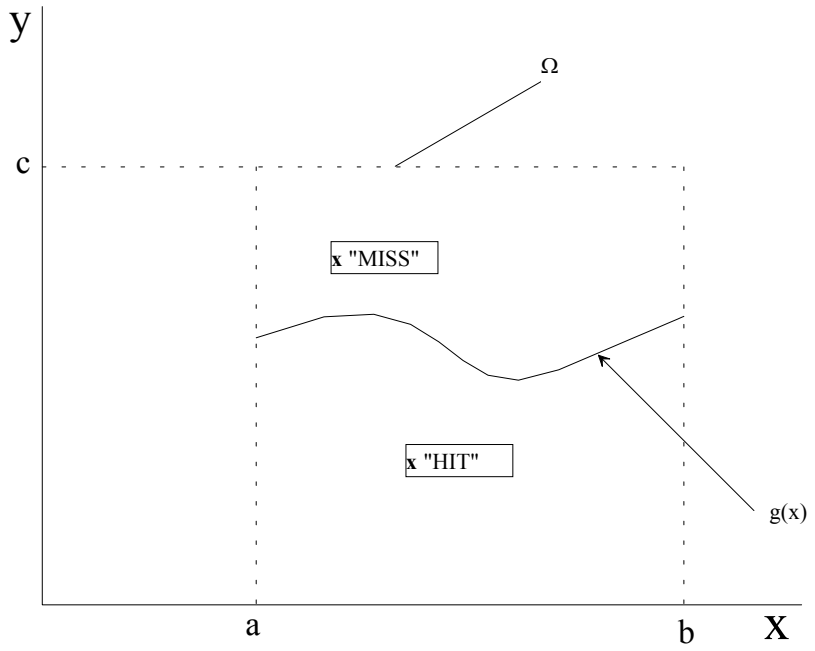

Figure 29. Monte Carlo Integration.

Let (X,Y) be a random vector uniformly distributed over the rectangle Ω with probability density function

$$f_{XY}(x,y) = \begin{cases} \dfrac{1}{c(b-a)} & if\ (x,y) \in \Omega \\ 0 & otherwise \end{cases}$$

The probability p that (X,Y) falls within the area under the curve g(x) can be written as

$$p = \frac{area\ under\ curve\ g(x)}{area\ of\ \Omega} = \frac{\int_a^b g(x)dx}{c(b-a)} = \frac{I}{c(b-a)}$$

If N independent random vectors (X_1,Y_1), (X_2, Y_2), …, (X_N, Y_N) are generated, the probability p can be estimated by

$$\hat{p} = \frac{N_H}{N}$$

Where N_H is the number of times $g(X_i) \geq Y_i$; that is, the number of "hits," as shown in Figure 29. From these two equations, we can estimate the value of the integral I as

$$I \cong c(b-a)\frac{N_H}{N}.$$

In other words, the value of the integral I is the fraction of points that lie under the curve defined by g(x) multiplied by the area of the rectangle Ω.

This thesis uses Monte Carlo integration to estimate two quantities: the packing density and the solid-void surface area.

C-2 Estimation of Packing Density

For a non-overlapping packing, the packing density can be computed exactly by adding up the volumes of all the particles and dividing this quantity by the volume of the region:

$$PackingDensity = \frac{4}{3}\pi \frac{\sum_{i=1}^{N} r_i^3}{(\mathrm{Re}\,gionRadius)^3}.$$

However, once the packing has been expanded, neighboring particles will overlap. Using the simple geometric technique just described will result in packing densities greater than unity, which are physically impossible. Once the packing has been expanded, the overlapping volume fractions of adjacent particles need to be taken out of the calculation (see Figure 30). This proved to be extremely difficult, so Monte Carlo integration was used to estimate the volumes of the particles.

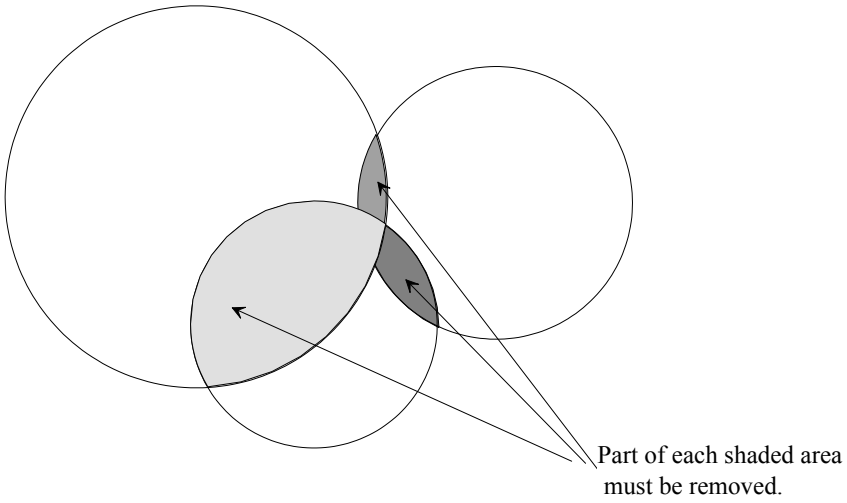

Figure 30. Overlapping Volume Fractions in the Density Calculation.

A uniform random sample of N data points is generated in the interval (-RegionRadius, RegionRadius). This region represents a cube of side 2*RegionRadius. All data points in the sample that were outside the spherical region of radius RegionRadius were removed from the sample, leaving a uniform random sample of data points in the spherical region of interest. See Figure 31.

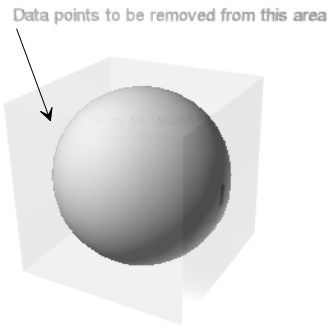

Figure 31. Cube with Inscribed Sphere.

The program considers each data point N_i in turn, checking whether it is inside the first particle in the Particles array (the Geometric Bounding Toolbox, described elsewhere in this thesis, includes a routine for doing this). If it is not, the program checks it against the next particle, and so on, until the point is inside a particle, or until it has been checked against all particles. The next data point is then considered, and so on, until all N points have been considered.

If the data point N_i is inside a particle, the Boolean variable IN is assigned a value of 1, the counter in* is incremented by one and the program moves on to the next data point. If the data point N_i is not inside any of the particles, the Boolean variable IN is assigned a value of 0.

Once all N data points have been checked against all particles, the packing density is estimated by $PackingDensity = \frac{in}{N}$. The algorithm for this routine is given in Figure 21.

This method was checked against the purely geometric method for several non-overlapping packings. It was found that an initial value of N = 100,000 data points produced a

* Variable names in MATLAB® are case-sensitive; IN, in and In are all different variables.

final value of N ≈ 52,000 data points (once the data points outside the spherical volume were eliminated) and generated an error relative to the geometric method of less than 1%. Increasing the initial value of N to 1,000,000 data points did not improve accuracy and significantly increased computation time.

C-3 Estimation of Solid-Void Surface Area

Computing the solid-void surface area involved identifying the fraction of each particle that was **not** intersecting any of the other particles, and computing the surface area of that fraction.

The surface area of a spherical segment is given in spherical coordinates by $S = R^2 \iint \sin\theta d\theta d\varphi$, with R, θ and φ defined as shown in Figure 32. For an entire sphere, the limits of integration are $0 \leqslant \theta \leqslant \pi$ and $0 \leqslant \varphi \leqslant 2\pi$, which reduces to the familiar $S = 4\pi R^2$. An incremental area unit dA is given by $dA = R^2 \sin\theta d\theta d\varphi$, for a constant R.

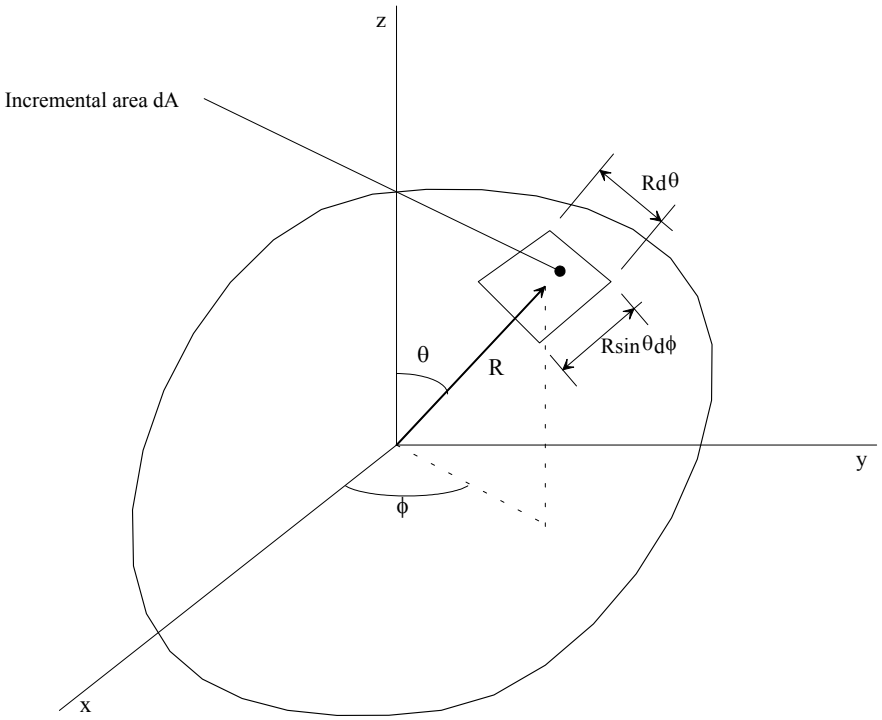

Figure 32. Incremental Area in Spherical Coordinates.

A uniformly distributed random sample of points N_i is generated on the surface of the i^{th} particle. These are generated in spherical coordinates (R,φ,θ) local to the particle. The coordinates of each point are transformed into Cartesian coordinates (x',y',z') local to the particle, and then into global Cartesian coordinates (x, y, z) (see Figure 33). The conversion from spherical to Cartesian coordinates is given by

$$x = R\sin\theta\cos\varphi$$
$$y = R\sin\theta\text{in}\theta\text{s}$$
$$z = R\cos\theta$$

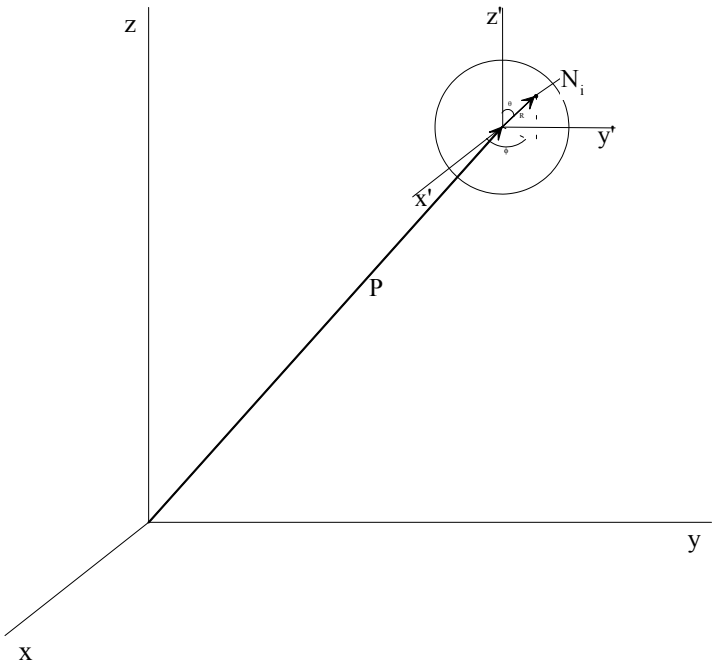

Figure 33. Local and Global Coordinates of Points on the Surface of a Particle.

Each of these data points is tested against the particles in contact with the particle under consideration (as given by the touch array, see Appendix A). If the point is in one of the contacting particles, it is not part of the solid-void surface. The Boolean variable SURF is assigned a value of 0, and the next data point on the surface is considered. If the point is not in **any** of the contacting particles, it is part of the solid-void surface, and the Boolean variable SURF is assigned a value of 1. The counter j is incremented by sinθ. The solid-void surface for the i^{th} particle is given by

$$SV_i = 2\pi^2 R_i^2 \frac{j}{N_i}.$$

Finally, the total solid-void surface area for the packing is given by

$$SVArea = \sum_{k=1}^{n} SV_k \ .$$

The algorithm for the solid-void calculation is given in Figure 27.

This method was checked against a geometric solid-void surface area calculation for various one- and two-particle models. It was found that values of $N_i \propto 100{,}000 R_i^{\,2}$ generated an error relative to the geometric method of less than 2%. However, the solid-void surface area became zero at less than 100% densification. Using more data points might overcome or mitigate this problem.

BIBLIOGRAPHY

BIBLIOGRAPHY

1. German, R.M., *Sintering Theory and Practice*. 1996, New York: John Wiley and Sons.
2. Ashby, M.F., *A first report on sintering diagrams.* Acta Metallurgica, 1974. **22**: p. 275-289.
3. Aigeltinger, E.H. and R.T. DeHoff, *Quantitative determination of topological and metric properties during sintering of copper.* Metallurgical Transactions A, 1975. **6A**: p. 1853-1862.
4. Kingery, W.D., H.K. Bowden, and D.R. Uhlmann, *Introduction to Ceramics*. Second ed. Wiley Series on the Science and Technology of Materials. 1976, New York: John Wiley & Sons. 1032.
5. Exner, H.E. and E. Arzt, *Sintering Processes*, in *Physical Metallurgy*, R.W. Cahn and P. Haasen, Editors. 1996, Elsevier Science: Amsterdam. p. 2628-2662.
6. Slaughter, W.S., et al., *A quantitative analysis of the effect of geometric assumptions in sintering models.* Acta Metallurgica, 1997. **45**(12): p. 5077-5086.
7. Baddeley, A., *Stereology*, in *Spatial Statistics and Digital Image Analysis*. 1991, National Academy Press: Washington, D.C.
8. DeHoff, R.T. and F.N. Rhines, *Quantitative Microscopy*. 1968: McGraw-Hill.
9. Smith, L.N. and P.S. Midha, *Computer simulation of morphology and packing behaviour of irregular particles, for predicting apparent powder densities.* Computational Materials Science, 1997. **7**: p. 377-383.
10. Nankadumar, K., Y. Shu, and K.T. Chuang, *Predicting geometrical properties of random packed beds from computer simulation.* AIChE Journal, 1999. **45**(11): p. 2286-2297.
11. Nolan, G.T. and P.E. Kavanagh, *Computer simulation of random packing of hard spheres.* Powder Technology, 1992. **72**: p. 149-155.
12. Patterson, B.R. and J.A. Griffin. *Effect of particle size distribution on sintering of tungsten*. in *International Powder Metallurgy Conference*. 1984. Toronto, Ontario: Metal Powder Industries Federation.
13. Patterson, B.R. and V.D. Parkhe. *Particle size distribution effects on sintering of spherical tungsten*. in *Annual Powder Metallurgy Conference*. 1985. San Francisco: Metal Powder Industries Federation.

14. Shiau, F.-S., T.-T. Fang, and T.-H. Leu, *Effects of milling and particle size distribution on the sintering behavior and the evolution of the microstructure in sintering powder compacts.* Materials Chemistry and Physics, 1998. **57**: p. 33-40.

15. Yeh, T.-S. and M.D. Sacks, *Effect of particle size distribution on the sintering of alumina.* Journal of the American Ceramic Society, 1988. **71**(12): p. C484-C487.

16. Ting, J.-M. and R.Y. Lin, *Effect of particle-size distribution on sintering Part I Modeling.* Journal of Materials Science, 1994. **29**: p. 1867-1872.

17. Ting, J.-M. and R.Y. Lin, *Effect of particle size distribution on sintering Part II Sintering of alumina.* Journal of Materials Science, 1995. **30**: p. 2382-2389.

18. Matheson, A.J., *Computation of a random packing of hard spheres.* Journal of Physics C: Solid State Physics, 1974. **7**: p. 2569-2576.

19. Smith, L.N. and P.S. Midha, *A computer model for relating powder density to composition, employing simulations of dense random packings of monosized and bimodal spherical particles.* Journal of Materials Processing Technology, 1997. **72**: p. 277-282.

20. Milne, S.J., M. Patel, and E. Dickinson, *Experimental studies of particle packing and sintering behaviour of monosize and bimodal spherical silica powders.* Journal of the European Ceramic Society, 1993. **11**(1): p. 1-7.

21. German, R.M., *Powder Metallurgy Science*. 1984, Princeton: Metal Powder Industries Federation.

22. Weisstein, E., *Log Normal Distribution*. 1999, Wolfram Research.

23. Zheng, J. and J.S. Reed, *Effects of particle packing characteristics on solid-state sintering.* Journal of the American Ceramic Society, 1989. **72**(5): p. 810-817.

24. Edwards, S.F., *Equations of granular materials.* Physica A, 1999. **274**: p. 310-319.

25. Krishnan, K., *Modeling Sintering in Ceramics*, in *Mechanical Engineering*. 2000, University of Pittsburgh: Pittsburgh. p. 130.

26. Nolan, G.T. and P.E. Kavanagh, *Computer simulation of random packings of spheres with log-normal distributions.* Powder Technology, 1993. **76**: p. 309-316.

27. Exner, H.E., *Principles of Single Phase Sintering*, in *Reviews in Powder Metallurgy and Physical Ceramics*. 1979. p. 7-251.

28. Nettleship, I., et al. *Dimensionless parameters for the analysis of sintering microstructures*. in *International Conference on Powder Metallurgy and Particulate Materials*. 1997. Chicago: Metal Powder Industries Federation.

29. Nettleship, I. and W.S. Slaughter, *Dimensionless parameters for microstructural pathways in sintering.* Journal of the American Ceramic Society, 1998. **81**(3): p. 700-704.

30. Veres, S.M. and D.Q. Mayne, *Geometric Bounding Toolbox, Version 7.2*. 2002.

31. Nolan, G.T. and P.E. Kavanagh, *The size distribution of interstices in random packings of spheres.* Powder Technology, 1994. **78**: p. 231-238.

32. Rubinstein, R.Y., *Simulation and the Monte Carlo Method*. Wiley series in probability and mathematical statistics. 1981, New York: John Wiley and Sons.